Fall 2021

Purification of Uranium Tetrafluoride Using Ammonium Bifluoride

Kyle Robert Foster

PURIFICATION OF URANIUM TETRAFLUORIDE USING AMMONIUM BIFLUORIDE

by

Kyle Robert Foster

Bachelor of Science
University of South Carolina, 2019

Submitted in Partial Fulfillment of the Requirements

For the Degree of Master of Science in

Mechanical Engineering

College of Engineering and Computing

University of South Carolina

2021

Accepted by:

Theodore Besmann, Director of Thesis

Josh Gray, Reader

Tracy L. Weldon, Interim Vice Provost and Dean of the Graduate School

ACKNOWLEDGEMENTS

I would like to extend my deepest gratitude to my primary advisor and thesis director, Dr. Theodore Besmann. Dr. Besmann not only secured funding for this work and strove to provide assistance directly whenever needed, but he put together a team of postdocs and students of the highest caliber in both knowledge and character. It has been an absolute privilege to be able to be a part of this team during my graduate schooling.

Specifically, I would like to thank Dr. Juliano Schorne-Pinto for his incessant willingness to help others. Further, I would like to directly acknowledge Dr. Mina Aziziha and Jacob Yingling for their frequent delaying of their own work in order to assist me with mine whether for discussions or assistance in the lab.

I would like to acknowledge Dr. Markus Piro, Dr. Bernie Fitzpatrick, and Ksenia Lipkina out of Ontario Tech University for our many discussions regarding our purification endeavors.

This research was supported by the U.S. DOE Office of Nuclear Energy, Nuclear Energy Advanced Modeling and Simulation Program and the Nuclear Energy Universities Program, project DE-NE0008985.

ABSTRACT

Molten salt reactors are being deployed as one of the Generation IV nuclear reactor concepts starting in 2025. While their applications and safety potential are considered extremely advantageous, there is a lack of operating history to draw on, so thorough understanding of proposed molten salt materials' thermochemical behavior is crucial to their successful implementation.

The most prominent fissile fuel proposed for molten salts is uranium tetrafluoride (UF_4) using ^{233}U of the thorium fuel cycle. UF_4 is extremely hygroscopic, meaning it will react with moisture and oxygen in its environment, so as-received powders contain significant levels of impurity. In order to have UF_4 for use in experimental thermochemical assessments of UF_4-containing binary and ternary systems, the powder must be purified prior to experimentation. In this work, a process for purification of as-received uranium tetrafluoride is developed using the solid-state reaction between ammonium bifluoride and uranium oxides at elevated temperatures. This process required the selection of a compatible reaction vessel, the creation of a KOH off-gas scrubbing system for the produced HF gas, and a reaction system as devoid of oxygen as possible to prevent further oxidation. Special attention had to be paid to materials interaction between the volatile gaseous products and system components at all points past the reaction vessel. The purification process and its results are explored using various experimental methods, including DSC, XRD, and TGA. Variables explored in

the process of purification optimization include powder ratio, ramp rate, and reaction time.

TABLE OF CONTENTS

LIST OF TABLES

LIST OF FIGURES

LIST OF ABBREVIATIONS

DSC.....Differential Scanning Calorimetry

DTA ..... Differential Thermal Analysis

GIF ..... Generation IV International Forum

ICP-MS ..... Inductively Coupled Plasma Mass Spectrometry

LWR.....Light Water Reactor

MSFR.....Molten Salt Fast Reactor

MSRE.....Molten Salt Reactor Experiment

MSR ..... Molten Salt Reactor

ORNL.....Oak Ridge National Laboratory

PTFE .....Polytetrafluoroethylene

SDS .....Safety Data Sheet

SS ..... Stainless Steel

TGA ..... Thermogravimetric Analysis

XRD ..... X-Ray Diffraction

CHAPTER 1: INTRODUCTION

Among the greatest discoveries of the 20th century was the ability to harness the energy created by fission, which became the basis of nuclear energy. Fission is the process of a heavy nuclei splitting into two fragments, known as fission products, and releasing large sums of energy in the process. When nuclei are unstable (particularly in specific heavy isotopes), they can decay spontaneously through radioactive decay, but this phenomenon can also be forced through neutron bombardment of certain materials' nuclei. Nuclear fission occurs when this neutron bombardment-forced nuclei splitting creates a chain reaction through the release of free neutrons which can strike another atom. The resulting atom is then one atomic unit heavier than its stable state, forcing another split into lighter nuclei [1,2]. Nuclear fuels, which are considered to be fissile, are able to sustain this chain reaction. The most common of these materials are ^{235}U and ^{239}Pu.

The splitting and repulsion of the fission process releases exorbitant amounts of energy in the form of heat, and nuclear power reactors utilize this heat via a transfer medium (coolant) to create a natural convectional flow, which is often assisted by a pump. The heated coolant goes through an external loop where, depending on the type of reactor, it either goes into a steam generator or heat exchanger (connected to a steam generator). The steam then is fed steam turbine where the heat will be converted to power [3,4].

This process is not reliant on fossil fuels, making it a near carbon-neutral energy solution [4]. Over the past decades, it has become abundantly clear that the world must reduce greenhouse gas and CO_2 emissions to combat global warming that is already spiraling out of control, as is evidenced by Figure 1.1 [5,6]. In the most recent statement by the Intergovernmental Panel on Climate Change in August of 2021[6], it was released that "it is unequivocal that human influence has warmed the atmosphere, ocean and land. Widespread and rapid changes in the atmosphere, ocean, cryosphere and biosphere have occurred". According to 2014 data released by the EPA[7], over 30% of the emissions contributing to this trajectory come from the burning of fossil fuels for use in energy production.

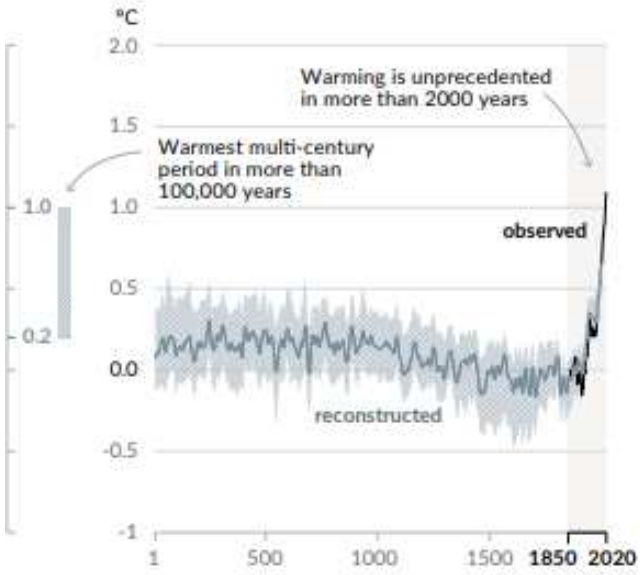

Figure 1.1: Shown is the change of the Earth's surface temperature as observed from 1850-2020 and reconstructed from years 1-1850. Copied from the IPCC 2021 Report for Policy Makers [6].

With the world's energy demands growing rapidly, efforts must be made to adopt a far larger share of renewable and carbon neutral power generation methods [5,8]. Fossil

fuels set the consumer-cost of electricity in most cases, which is one of the primary obstacles nuclear power has to overcome to see mass adoption. Along with this, nuclear must overcome safety concerns (largely public opinion which makes it not politically advantageous to be a proponent of), grid appropriateness (ability to meet demands), waste concerns, and security concerns (state-sponsored weapons proliferation) [9,10]. Despite this, nuclear power shows significant future promise and provided 2553 TWh of electricity in 2020 worldwide [4]. The historical path of its adoption can be seen in Figure 1.2.

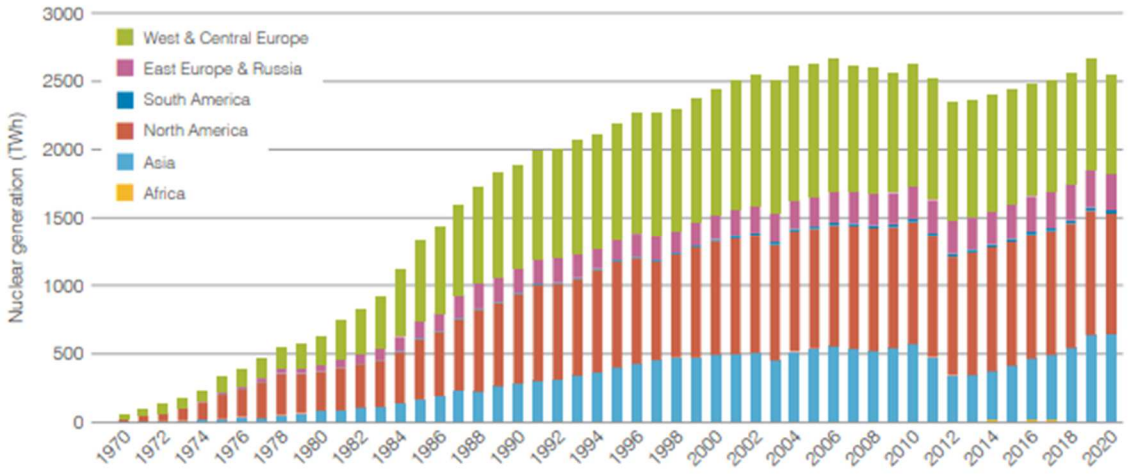

Figure 1.2: Nuclear electricity generation from 1970 to 2020 in TWh. Copied from World Nuclear Performance Report 2021 [4].

The near exponential growth of the industry in its early years has since slowed down significantly despite global calls for non-carbon based electricity generation growing. Public perception has been a long-standing problem within the nuclear field, and plays a strong role in this decline, particularly following 2011's Fukushima accident [4,10]. The other major contributing factor was the startup costs of building novel reactors due to the lack of established processes that typically work to continually drive down industry costs. These concerns, among the others facing nuclear energy, were addressed

by the selection of 6 promising concepts to concentrate efforts on for the future of the nuclear field by the Generation IV International Forum in 2002 [9,10].

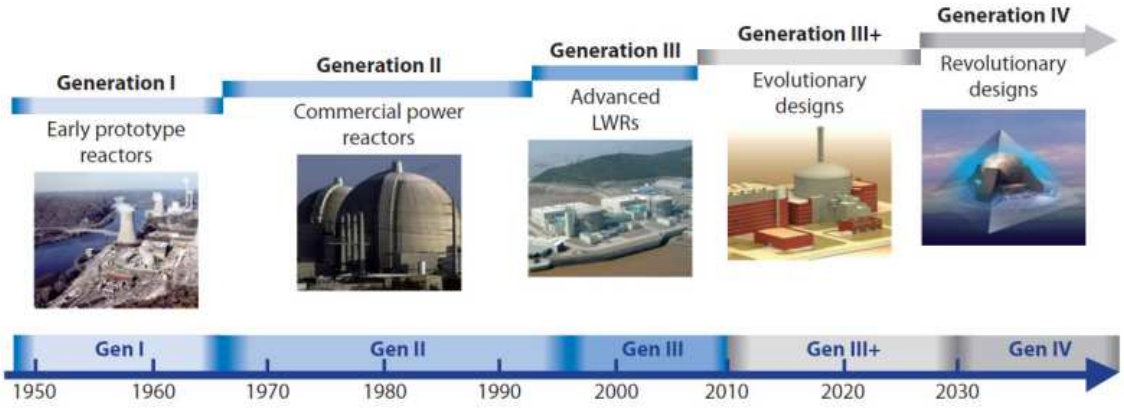

Figure 1.3: The generations of nuclear power plants are shown with generation 1 being made of experimental reactors, generation 2 being made up of commercially deployed reactor types (such as PWRs, BWRs, and CANDU reactors), generation 3 being primarily efficiency, safety, and construction improvements on generation 2, and generation 3+ incorporating further safety improvements on the previous generation. Copied from Technology Roadmap Update for Generation IV Nuclear Energy Systems [10].

Generation IV reactors were chosen on sustainability (in terms of waste and fuel utilization), economics, safety, and reliability [9,10]. The goal of the program was to concentrate global efforts on agreed upon concepts to allow for faster, easier, and cheaper deployment, improved collaboration in research, and increased competitiveness of the proposed reactor types. Each concept was to go through a viability phase, a performance phase, and a demonstration phase [9,10]. The concepts selected for these efforts were:

- Gas-Cooled Fast Reactor;
- Lead-Cooled Fast Reactor;
- Sodium-Cooled Fast Reactor;
- Supercritical-Water-Cooled Reactor;
- Very-High-Temperature Reactor;

- Molten Salt Reactors.

CHAPTER 2: THESIS OBJECTIVES

There is great interest within the nuclear field regarding the use of molten salts as both a medium for heat transfer within solid fuel reactors and a basis for the Generation IV Forum-selected concept of molten salt reactors. As such, understanding thermophysical properties of the proposed salts for use is essential to understanding these types of reactor's behavior. The University of South Carolina has been sub-contracted by Los Alamos National Laboratory to create a molten salt thermophysical property database to assist in filling this need. The work within this thesis is in support of the creation of this database so accurate experimental measurements of systems containing uranium tetrafluoride can be conducted.

The overarching goal of this thesis is to purify as-received uranium tetrafluoride using ammonium bifluoride to avoid the costly and hazardous inclusion of a HF gas line in our laboratory. While this concept has been published on before, the literature surrounding the process contains many inconsistencies and omissions that result in significant complications when trying to reproduce. Because of this, the other main goal of this thesis is to document the process and system used to purify uranium tetrafluoride in such a way that will be reproducible for both our own university and other universities for the betterment of the molten salt community.

It is well-documented that salts in their as-received state require purification processes to remove impurities formed during transport to produce accurate and reproducible experimental data [1,11–14]. Actinide salts in particular are susceptible to the

formation of impurities due to the stability of both oxides and oxyfluorides at standard temperature and pressure. The DSC curve shown in Figure 2.1 is of as-received uranium tetrafluoride provided to our university by ORNL. While we do not have a way of knowing the extent of impurities of the received salt, it is likely impurities are present as shown by the peak present at 923.5˚C and observed instability of the DSC curve on closer analysis (shown in Figure 2.2). Based on literature, the DSC curve for uranium tetrafluoride should possess a peak at 1034-1036˚C and be smooth until that point [15].

The curve shown in Figure 2.1 will act as a baseline for the as-received uranium tetrafluoride, and improvement upon this, will indicate completion of the main objective of this thesis.

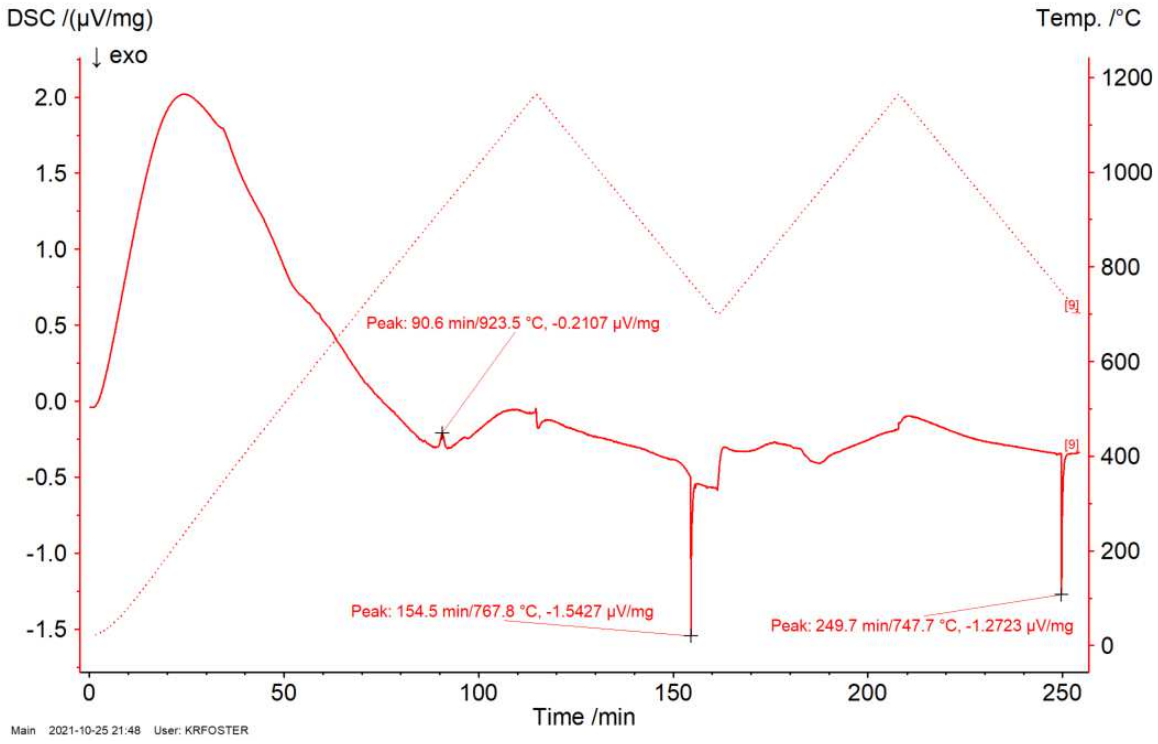

Figure 2.1: Initial DSC run on UF_4 provided by ORNL showing a peak on initial heating of 923.5˚C.

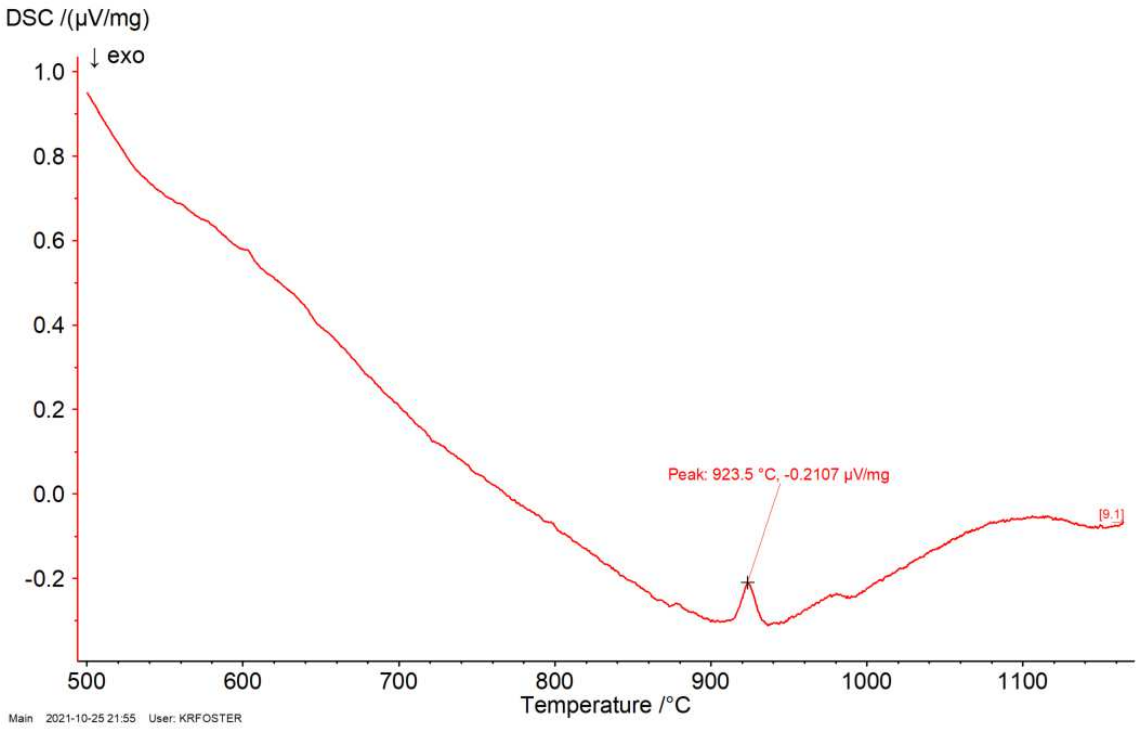

Figure 2.2: Stripped down DSC curves obtained from initial heating of ORNL-sourced UF_4.

CHAPTER 3: MOLTEN SALT REACTORS

Molten salts are of have been a topic of significant interest within the nuclear field dating back to the late 1940s [1,3,9,16–19]. Molten salts, in particular fluorides, possess significant advantages as a heat transfer medium within a reactor when compared to water as a result of their high volumetric heat capacity, high boiling point, and chemical inertness [1,11,18,20,21]. In addition, molten salts offer major improvements with regards to safety when compared to traditional reactor mediums (pressurized water). Their potential for low operating pressure, which is near atmospheric, drastically reduces the chances of a significant accident due to the role that high pressures play in radioactivity release during nuclear meltdowns. Molten salts' liquid state also opens the possibility of passively draining a reactor in the case of an incident. If the drained salt is fissile, the dump tanks can be designed in such a way that renders the fuel subcritical. This possibility would drastically reduce a reactor's overheating risk [1,16,17]. Due to the favorable properties and the potential of molten salts, an entire new concept of reactor was created around them called molten salt reactors.

Molten salt reactors are a subset of nuclear fission reactors characterized by their use of a molten salt mixture as the reactor's primary coolant. There are two subclasses that have been theorized within this reactor concept which are separated by whether or not fissile fuel is in the form of a molten salt. The subclass of molten salt reactors for which this thesis more directly pertains to are reactors in which the fissile fuel is dissolved into a molten salt matrix being used as a medium between the reactor's heat

exchanger and reactor core. There are many significant advantages to a molten fuel. One of the primary draws of this concept is the allowance of continuous online reprocessing during which fission products can be removed and replaced with fissile actinide materials [1,9–11,17,21–23]. This online removal of fission products allows for a higher fuel burn-up, increased reaction speed, as a result of decreased parasitic neutron capture effects of fission products, and shorter-lived radioactivity among the waste [23]. The increased efficiency experienced as a result of the removal of fission products allow for significantly lower fissile inventory required to begin operation when compared to traditional reactor types [16–18].

There were originally two main subcategories for this type of reactor, which are the one fluid design and the two fluid design. One fluid design reactors faced considerably less feasibility concerns while still possessing the advantages of using molten salt as both the fuel and the transfer medium, so over time, the two fluid designed was abandoned. In the one fluid concept, the liquid fuel acts as the reactor coolant and circulates throughout the entire core and vessel [1,11,12,16–18]. One of the most prominent types of one-fluid molten salt reactor being researched currently is the molten salt fast reactor (MSFR). This type of reactor can be used as a breeder reactor using the ^{233}U/thorium fuel cycle when combined with continuous parasitic fission product removal [15,21,23]. This is particularly attractive due to the supply limitations on conventional ^{235}U which is projected to last for approximately 80 years based on current consumption [24]. For this purpose, non-moderated (fast) reactor spectra are preferred over thermal spectra ones because the resulting nuclides have much higher energy (making all actinides fissionable) [15–18]. This results in a much higher fission to capture ratio than that of

thermal spectrum reactors [1]. In Figure 3.1, a generalized one fluid reactor with all necessary components for operation and online reprocessing is shown.

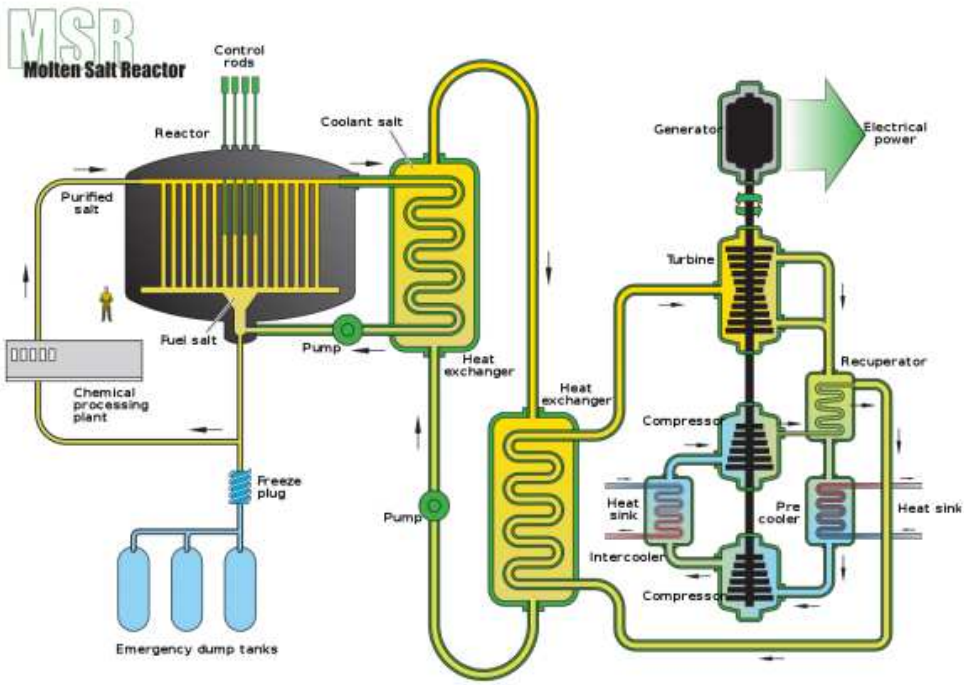

Figure 3.1: Single fluid reactor design with necessary components for fuel reprocessing. Copied from U.S. Department of Energy Research Advisory Committee [9].

The fuel used for molten salt reactors is composed of a molten halide salt with an actinide halide salt dissolved in it. The salt used is heavily based upon physical characteristics, such as melting point, and how readily the fissile material dissolves into the salt. Fluoride salts tend to fit the necessary parameters the best, and they are, therefore, the most extensively researched and utilized type of salt [12,15,17,18]. Chloride salts are also being explored, however, despite their higher vapor pressures and lower stability at high temperatures due to their less aggressive nature and lower melting points [15,17,18]. Chlorides can be used only in fast reactors however, not thermal ones, due to the chlorine

atom's large neutron-capture cross-section [1,15]. This, combined with their lack of operating history to draw on, makes them less favorable than fluorides at this point.

Despite the community's preference for fluorides, they do have a significant drawback in their propensity for severe corrosion. As a result of this, material selection for reactors can be problematic, and it is important to use materials that have resistance to melting into fluoride mixtures. Nickel-based alloys are the most frequently used materials for this purpose due to their resistance to reaction, resistance to radiation, and high temperature capabilities. Diffusive barriers from the alloy materials are also key in resisting corrosion by the creation of surface films that prevent outward diffusion of alloy materials. For this purpose, chrome and aluminum are often included in Ni-based alloys used with molten salts to provide resistance to oxidation [1,3,11,17,18,20,25]. One example of this is the Ni-based alloy Hastelloy N, with 7% Cr. This alloy was created by ORNL specifically for use with molten salts and allows safe operation temperatures up to almost 1000 centigrade [11,20,25]. This is the most common alloy used when working with molten salts due to its carefully selected properties and resistance to reaction.

Historically, ORNL has acted as the primary research laboratory on molten salt reactors, and their efforts resulted in a proof-of-concept reactor, known as the Aircraft Reactor Experiment, in 1954 and an 8 MW operational research reactor, known as the Molten Salt Reactor Experiment, in 1965. However, ORNL's attention shifted away from MSR's in the mid-1970s as a result of a shift of the Atomic Energy Commission's focus to liquid metal fast breeder reactors [1,3,12,17].

In 2002, interest returned for MSRs following their selection as one of the six promising future concepts for the Generation IV initiative [1,3,9,10,16,17]. Many types of

reactors have emerged as subjects of interest involving molten salts since this time, with some involving the traditional thermal-spectrum and others involving a fast-spectrum. These fast-spectrum designs often utilize chlorides as their base, and they have the ability to maintain a higher breeding ratio than previous concepts [3,15,17,20,23]. Less traditional forms of reactors involving molten salts have also emerged as topics of interest for nations around the world where molten salts simply act as coolants for solid fuel elements, known as molten salt cooled reactors or advanced high temperature reactors [1,3,17].

Many obstacles that faced the molten salt community in its infancy are no longer as big of concerns. Significant advances in experimental techniques, such as differential scanning calorimetry, and computational methods, such as the modified quasi-chemical model, have allowed far more accurate and obtainable literature surrounding salt properties. However, there is still far more work to be done in the field of molten salt thermodynamics due to intricacies faced in experimental work stemming from their hygroscopic and reactive nature. This tendency to react causes impurity concerns, leading to uncertainty in many existing measurements [1,3,11,12,18].

CHAPTER 4: LITERATURE REVIEW

The literature review within this chapter contains sections on uranium behavior, synthesizing actinide fluorides, purifying actinide fluorides, and materials interaction. The sections on purification and synthesis of actinide fluorides are separated despite their similarities due to the inability to compare their results directly due to different starting materials. While important information can be drawn from papers on synthesis of actinide fluorides from actinide oxides, work on purification can be more directly drawn from in this thesis. The purpose of this literature review was to gain an in-depth understanding of existing literature on the topics that will be explored within this thesis.

4.1 Uranium Behavior

Literature surrounding UF_4's transition temperatures contain significant discrepancies. Papers up to the early 2000's attribute a melting point of 960˚C to UF_4[26,27], while other papers, with dates ranging from 1961 to present recognize a melting point of 1036˚C (although Soucek et al. indicate a slightly different value of 1034 from their own work[15]) [28,29]. In a series of papers involving UF_4 binaries out of the Soviet Union in the 1960s [13,30], a phase transition was identified for UF_4 at 841˚C. This transition is not consistent with any data prior or since, but it is also the only published literature on UF_4 that gathered its data both from DTA on both heating and cooling. Very little explanation of this novel transition was coherent following the papers' translation from Russian to English for this work, but presumably this transition was a result of cooling data inclusion.

In response to this novel transition being reported, Dworkin out of ORNL[30] revisited the thermochemical behavior of UF_4 (with observed .7 mole percent UO_2) by measuring enthalpy from room temperature to above the compound's melting point. In this work, no indication of the transition at 841˚C was observed. It is suggested that while Khripin et al. address and mitigate oxidation concerns, they could still possess cation impurities. The suggested cause for this observed phase transition was the presence of calcium within their melt due to the known eutectic at 843˚C in the UF_4-CaF_2 system[30].

For the purposes of this thesis, most uranium tetrafluoride impurities were considered to be UO_2, but it is important to consider other impurity possibilities. The use of staged heating allows oxygen to fully be removed prior to temperatures being increased to combat the formations of uranyl difluoride when using ammonium bifluoride [27]. This impurity was shown to be particularly stable in the work of Pomiro et al., but according to Le Chatelier's principle, uranyl difluoride can be reduced to form UF_4, water, and oxygen in systems when exposed to HF in environments with partial pressures of O_2 and H_2O below 10^{-3} atm [31]. In the unlikely event of UO_3 impurities, UF_4, H_2O, and O_2 were shown to be the favored products in temperatures below 235˚C in a reaction with HF.

The reaction of U_3O_8 and ammonium bifluoride was shown by Wani et al. to form $[NH_4]_3UO_2F_5$ [32]. There is little published literature on this compound, but in the case of Th, Y, Pu, and other U oxides, on heating, similar salts that were formed release one ammonium fluoride at a time [24,27,33,34]. If this was consistent with U_3O_8 and ammonium

bifluoride, the reaction would presumably lead to uranyl difluoride, which can be reduced with HF at sufficiently low pressures[31].

4.2. Synthesizing Actinide Fluorides

The extreme hygroscopic tendencies of actinide fluorides pose significant complications with regards to transportation. Beyond this, oxides tend to be the most easily accessible forms of actinide materials, so there is extensive literature surrounding synthesis of actinide fluorides from their as-received oxide states dating back as far as the 1940s. At this time, a significantly different method of synthesis was used compared to more recent literature. Booth et al.[35] produced uranium tetrafluoride by flowing freon-11 and freon-12 over uranium trioxide targeting the following two equations, with the first being for freon-12 and the second for freon-11.

Freon-12 at 400˚C:

$$2CF_2Cl_2 + UO_2 \rightarrow UF_2 + CO_2 + COCl_2 + Cl_2 \qquad \text{Equation 4.21}$$

Freon-11 at 360-380˚C

$$4CF_2Cl_2 + UO_3 \rightarrow UF_2 + CCl_4 + COCl_2 + Cl_2 \qquad \text{Equation 4.2}$$

While it seems unlikely that the impurities present within our UF_4 are uranium trioxide, they remain unidentified, so it is important to consider all possible reaction paths that would result in pure UF_4.

Over 40 years later, Wani et al.[32] explored the reactions between 9 different binary oxides and ammonium bifluoride. Of the most important for the purposes of this thesis were the oxides U_3O_8 and UO_2 which at room temperature reacted to form $(NH_4)_3UO_2F_2$ (yellow powder) and $(NH_4)_4UF_8$ (green powder), respectively. This

reaction between UO_2 and ammonium bifluoride is supported through several other sources of published literature, but the reaction with U_3O_8 appeared to be novel at the time and unexplored in more recent publications [24,27,36]. Several unique characteristics were brought to light within this paper regarding these reactions. One of which was that mass transport acted unidirectionally from ammonium bifluoride to the oxides, and even following a week of contact, there was no reaction into the ammonium bifluoride rod in contact with the oxides. Another characteristic of this reaction was the necessity of water in the reaction which resulted in the author questioning whether this was truly a solid-state reaction or if the water is the medium of transport over the materials' interfaces. Reactions mixed under vacuum would not react over any period of time, but when allowed to pull moisture from the air, even for a few seconds, the reaction could proceed to completion [32]. The kinetics of each reaction were also observed, and the reaction of UO_2 was found to be slow, at a rate of ~50 Å sec^{-1}, as opposed to the faster reaction of U_3O_8, at a rate of ~200 Å sec^{-1}.

The synthesis of UF4 using ammonium bifluoride can be found over a large variety of sample sizes in literature. The largest observed use of this method comes from Charles Yeamans' master's thesis from MIT in 2003[27], where he allowed 44.8 g of ammonium bifluoride to react with 52.4 g of UO_2 in air over 17 days, stirring occasionally. He also ran another mixture of the same molar concentrations through a ball mill for 20 min and compared the speed of reaction between the unagitated and the agitated samples. The ball milled samples reacted much faster than the occasionally manually stirred samples, indicating improved reaction kinetics with smaller particle sizes. The mixture left for 17 days was taken to 110˚C after analysis, and at this point,

the reaction was shown to proceed rapidly. For the total reaction to proceed to UF4, Yeamans determined that of the most importance was the peak temperature reached. All samples reacted fully to form UF_4 at a temperature of above 400˚C even if the temperature was dropped upon reaching a peak of over 400˚C rather than dwelled. The full reaction path was analyzed by TGA was shown to proceed based on the reaction process described by equations 4.3 to 4.8 as shown in Figure 5.5 of his master's thesis [29].

$$NH_4HF_2 + UO_2 \rightarrow (NH_4)_4UF_8 * H_2O \quad \text{Equation 4.23}$$

$$(NH_4)_4UF_8 * H_2O \rightarrow (NH_4)_4UF_8 + H_2O \quad \text{Equation 4.24}$$

$$(NH_4)_4UF_8 \rightarrow (NH_4)_3UF_7 + NH_4F \quad \text{Equation 4.25}$$

$$(NH_4)_3UF_7 \rightarrow (NH_4)_2UF_6 + NH_4F \quad \text{Equation 4.26}$$

$$(NH_4)_2UF_6 \rightarrow NH_4UF_5 + NH_4F \quad \text{Equation 4.27}$$

$$NH_4UF_5 \rightarrow UF_4 + NH_4F \quad \text{Equation 4.28}$$

When looking at successful fluorination using ammonium bifluoride, the initial mixture is always allowed to react at room temperature or a low dwell period before the temperature is ramped up. Some insight as to why this is comes from the work of Mukherjee et al.[34] in 2011 through their formation of YF_3 by the reaction of ammonium bifluoride and Y_2O_3. This work looked at room temperature reactions that had been allowed to occur over various lengths of time before being taken to a temperature of 275-375˚C under nitrous flow. The trial of most interest was the direct heating of the mixture without allowing the solid-state reaction for an extended period. This sample produced a final product of yttrium oxyfluorides [34]. This shows the present oxygen molecules will

not be removed from the reaction without the allowance of the solid-state reaction. This results in further stable impurities in the product salt.

Claux et al.[21] in their work with PuO_2 employed a slightly different method using ammonium bifluoride than the other sources in this section. They targeted fluorination using the gaseous HF produced by the dissociation of ammonium bifluoride beyond its melting point. There initial ramp was to 350˚C where the sealed crucible containing the mixture was allowed to dwell for 17 hours. There were two subsequent runs at 355˚C for 18 hours and 505˚C for 12 hours to remove experienced intermediate states and residual ammonium bifluoride that did not escape the sealed vessel at its elevated pressure of 300 bars. This method was found to create the correct final product, but analysis using an ICP-MS revealed the presence of 8% corrosion impurities in the form of NiF_2 and FeF_2 [21]. This type of impurity introduction is far from desirable, especially when compared to the over 99% pure samples created by the previously discussed methods.

Table 4.1 summarizes some of the literature available on the topic of fluorination of actinide oxides. The research for this thesis concentrated on literature using ammonium bifluoride mostly, but there is a wide range of literature available using the gaseous fluorination method using HF gas as shown by Soucek et al[15]. These methods present significant hazardous risks due to their direct use of HF within the lab which would ideally be avoided. This method has been proven quite effective, however, and Soucek et al.[15] found no remaining oxides present following two runs of the oxide under HF at 450˚C.

Table 4.1: Summary of Literature of Actinide Oxide Fluorination [15,21,24,27,32,34,35,51]

Starting Material	Ending Material	Environment	Heating Structure	Reaction Method	Listed Intermediates	Reference Number
UO_3	UF_4	Closed system first flown with oxygen and then with freon-11/freon-12	Electric resistance furnace taken to a temperature of above 400˚C for freon-12 and 360˚C-380˚C for freon-11	Gaseous flow of freon-11/freon-12	None	[35]
U_3O_8	$(NH_4)_3UO_2F_2$	Pellet in Pellet and rod in powder	Reacted at room temperature	Ammonium bifluoride in various ratios	$(NH_4)_3UO_2F_2$	[32]
UO_2	$(NH_4)_4UF_8$				$(NH_4)_4UF_8$	
UO_2	UF_4	Fluidized bed or stirred bed in Ar	Heated to 425˚C by either fluidized bed or stirred bed	Ammonium Bifluoride	In Order: $(NH_4)_4UF_8*H_2O$ $(NH_4)_4UF_8$ $(NH_4)_3UF_7$ $(NH_4)_2UF_6$ NH4UF5	[27]
Y_2O_3	YF_3	Kept at room temperature in plastic bags	Heated by TGA to 400˚C for up to 45 min	Ammonium bifluoride in 1:1, 3:1, 4.5:1, and 6.5:1 molar ratios $(NH_4)_4HF_2$:Y_2O_3	In order of highest to lowest molar concentrations: $(NH_4)Y_2F_7$ $(NH_4)_3Y_2F_9$ $(NH_4)_3Y_2F_9$ $(NH_4)_3Y_2F_9$	[34]
PuO_2	PuF_3	Closed Vessel in Glovebox (Ar)	Ramp to 350C over 3 hours with a 17-hour dwell period. Allowed to cool then heated to 355 C for 18 hours. Ramped to 505 C and held for 12 hours.	Ammonium bifluoride method in a (1:3 molar ratio PuO_2:NH_4HF_2	$(NH_4)_2PuF_6$	[21]
UO_2	UF_4	Closed vessel evacuated to a pressure of 1 mbar in a glovebox under Ar	Gas flown over for 20-60 min at 450˚C	Gaseous fluorination with HF gas	None	[15]
ThO_2	ThF_4		Gas flown over for 20-60 min at 600˚C			
ThO_2	ThF_4	Welded Ni capsule in Ar glovebox	Gas flown over for 20-60 min at 600˚C	Gaseous fluorination with HF gas	None	[51]
ThO_2	ThF_4	Mixed under hood at room temperature and reacted in a vacuum. Heated under Ar Flow.	Heated to 450C-750C	Ammonium bifluoride in mole increments of .5 from 1:4 to 1:6 Oxide:$(NH_4)_4HF_2$	$(NH_4)_3ThF_7$ for ratios 1:5 and higher $(NH_4)_4ThF_8$ for 1:4.5 and below	[24]

4.3. Purifying Actinide Fluorides

Thermodynamic measurements are inherently extremely susceptible to uncertainty caused by miniscule composition changes of a material. Looking at any phase diagram shows the extent of this, as small compositional changes can result in vastly different stability regions. The extent of the general reactivity of molten salts has become much more of a focus in recent years. This is evidenced by the work of Friedman et al. from 1962[14] referring to actinide tri- and tetrafluorides as not hygroscopic, however, that paper still describes the efforts that were gone through to ensure purity. This new understanding and emphasis mean much of the work done surrounding molten salt thermodynamic properties and measurements currently is being done to remove this uncertainty from existing data.

Even more so than regular molten salts, purification is vitally important with actinide fluorides due to the stability of the materials' oxides at standard temperature and pressure. Evidence of this can be seen in Figure 2.1 which show the DSC curves of as-received UF_4 supplied to our lab that was considered over 99% purity. While the samples may be >99% purity when shipped, it is clear to see that these curves possess significant impurities. It is likely these impurities are a result of shipping environments, but such transportation complications are unavoidable unless the material is to be made in-house for each use.

Less published literature is available on purifying actinide fluorides than synthesizing them from oxides, but there are still several occurrences of it being done successfully. In 1962, Benz et al.[36] reacted UF_4 with NH_4F as a means of exploring intermediate products between the reactants and purifying their as-received materials.

They dehydrated both the ammonium fluoride and the uranium tetrafluoride prior to their mixing in a 1:2 mass ratio of ammonium fluoride:UF_4. The observed pathway, as identified by XRD, shows the formation of $(NH_4)_4UF_8$ up to 130˚C in air. This is followed by the formation of $(NH_4)_2UF_6$ up to 180˚C which releases an ammonium fluoride to β-NH_4UF_5 in a vacuum. This compound forms NH_4F*3UF_4 up to 400˚C where it is reduced to UF_4 in a vacuum [38].

The reaction path described has slight discrepancies with that of Yeamans[27]. This is likely a result of the use of ammonium fluoride rather than ammonium bifluoride, but the consistencies between the two are found in that they both allow a long dwell for the initial solid-state reaction to form $(NH_4)_4UF_8$ in air and later NH_4UF_5 prior to forming UF_4. Even more importantly, they both fully proceed by 400˚C following a series of intermediate double salts due to the loss of individual ammonium fluoride molecules. Benz et al.[36] also provided visual descriptions of various intermediates that occurred, and these descriptions can be found in Table 4.2. These exact intermediates are dependent on proper stoichiometric ratios, however, from previous literature, it is shown that overshooting of these stoichiometric ratios should result in the same final product with a slightly varied reaction path [27,36]. These visual descriptions were corroborated by Penneman et al. [37] in their paper exploring the ammonium fluoride-uranium tetrafluoride-water system.

Table 4.2: Visual Description of Intermediates

Compound	Appearance	Stable Region
$(NH_4)_4UF_8$	Fine crystals- Pea green Large Crystals- Emerald Green	In air: 60-90˚C
$(NH_4)_2UF_6$	Fine Crystals- Blue Green	In air: 110-130˚C
$7NH_4F*6UF_4$	Fine Crystals- Light Green	In helium: 200-220˚C Under Vacuum: 150-170˚C
α-NH_4UF_5	Fine Crystals- Light Green	Under Vacuum: 80-200˚C with deficient NH_4F levels
β-NH_4UF_5	Fine Crystals- Green to blue-green	Under Vacuum:180-210˚C
γ-NH_4UF_5	Fine Crystals- Light blue-green	Under vacuum: 150˚C
NH_4F*3UF_4	Fine Crystals- Green	Under vacuum: 270-400˚C

A description of ORNL's actinide sample preparation method reveals the use of ammonium bifluoride for actinides that is not described in any of the other observed literature. They used a vessel, shown in Figure 4.1, heated in a pot furnace until the ammonium bifluoride reached a liquid state, and the temperature was held at this point for at least one hour before being ramped to higher temperatures [14].

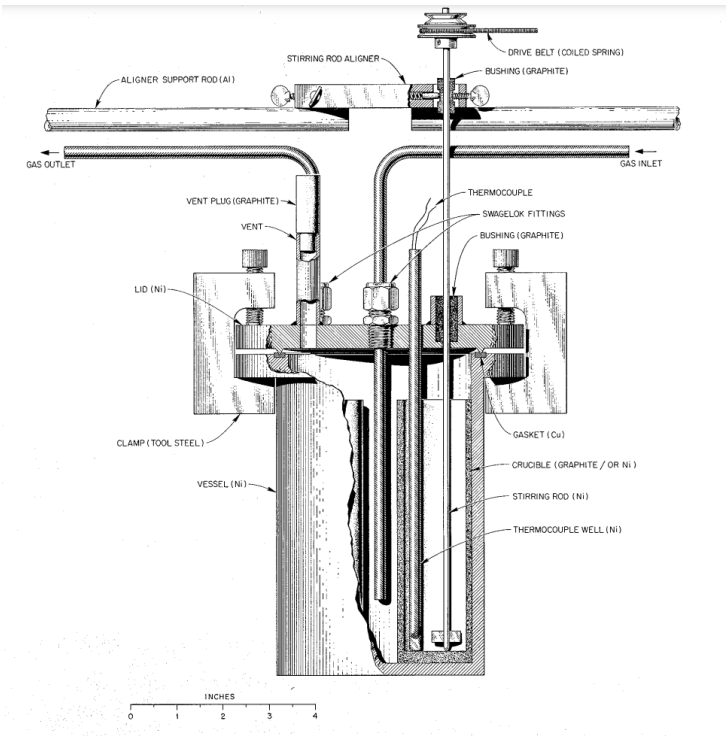

Figure 4.1: Reaction vessel used by ORNL within a pot furnace for the purification of actinide fluorides. The vessel was vented to allow for the removal of gaseous products during heating. Copied from Friedman et al [14].

The most recent occurrence of a successful purification method is from Elisa Capelli out of Delft University of Technology in 2015 [19]. Her work followed a very similar process to that of Claux et al.[21] described in section 4.2. She targeted the following two equations to remove oxide impurities from her ThF_4 [19].

$$NH_4HF_2 \rightarrow NH_3 + 2HF \qquad \text{Equation 4.9}$$

$$ThO_2 + 4HF \rightarrow ThF_4 + 2H_2O \qquad \text{Equation 4.10}$$

In a sealed Ni vessel, a mixture of undisclosed proportions of ammonium bifluoride and ThF_4, with presumed oxide impurities, was taken to 523 K for 12 hours in a furnace flown with Ar/H_2. Two subsequent runs were set at 673 K for 3 hours each to remove residual ammonium bifluoride and water [19]. As this was not the central portion

of her dissertation, many details within this were not disclosed making it hard to be sure what path this reaction took. However, the initial dwell temperature is just above the boiling point of ammonium bifluoride (512 K) in a sealed vessel, so the most likely path is the targeted reaction shown by equations 4.9 and 4.10. Others that followed this path experienced corrosion product impurities from the HF and surrounding materials (NiF2 and FeF2), so it is unclear how this was avoided[21]. With the container being sealed, any oxygen reacted off would not be able to escape, and on cooling would most likely form oxyfluorides or oxides. The most likely occurrence is that at the experienced pressures, the vessel was no longer sealed and allowed water vapor to escape. Subsequent runs would likely react off residual water that had not yet reacted with the product and could possibly even follow the solid-solid reaction with ammonium bifluoride for remaining impurities. More information would be needed on this endeavor to draw full conclusions, but her results are shown to be quite positive with regards to purity as shown in Figures 2.1 and 2.2 of her dissertation.

Hallatt, out of Ontario Tech University, followed a similar path to Capelli in his master's thesis [11]. The mixture targeted a molar ratio of 1:5.5 ThO_2:NH_4HF_2. He used stacked nickel crucibles for this purpose with the top crucible containing NaOH to react out gaseous HF produced. The top crucible fit into the bottom crucible as shown in Figure 4.2 and a lid, held in place by a weight, was placed on the upper crucible to provide sealing.

Figure 4.2: Stacked Ni crucibles used by Hallatt in purification endeavors. The top crucible possessed NaOH and had a weight placed on the lid when in use. Copied from Hallatt [11].

The entire reaction was carried out in an argon filled glovebox, and heating was provided by a hotplate with a sand-filled beaker containing the crucibles. The hotplate was set to 350˚C for 12 hours, resulting in a temperature of around 250˚C at the crucible due to thermal lag. The result was measured by XRD and possessed a peak at 28.23˚ that should not have been present in ThF_4, but it was concluded that this peak was present upon receiving the ThF_4 and was not a product of the purification procedure [11]. It seems likely that this was in fact a peak from a thorium oxyfluoride that was reported by Bahri et al at 28.39˚.

Lipkina[12], also out of Ontario Tech University, initially followed the same process as Hallatt while varying mass ratios used. She eventually switched to following Capelli's method within a sealed Netzsch DSC crucible that was qualified as leak tight up to 1200˚C. Her method involved an initial heat treatment of 250-350˚C for 12 hours followed by a dehydration stage at 400˚C for 6 hours. This method, which was almost exactly the same as the successful method out of Delft, was found to be unsuccessful using DSC runs (shown in Figure 4.3). While the locations of observed peaks are not disclosed, the initial melting peak appears to occur significantly below the theoretical value of 1110˚C.

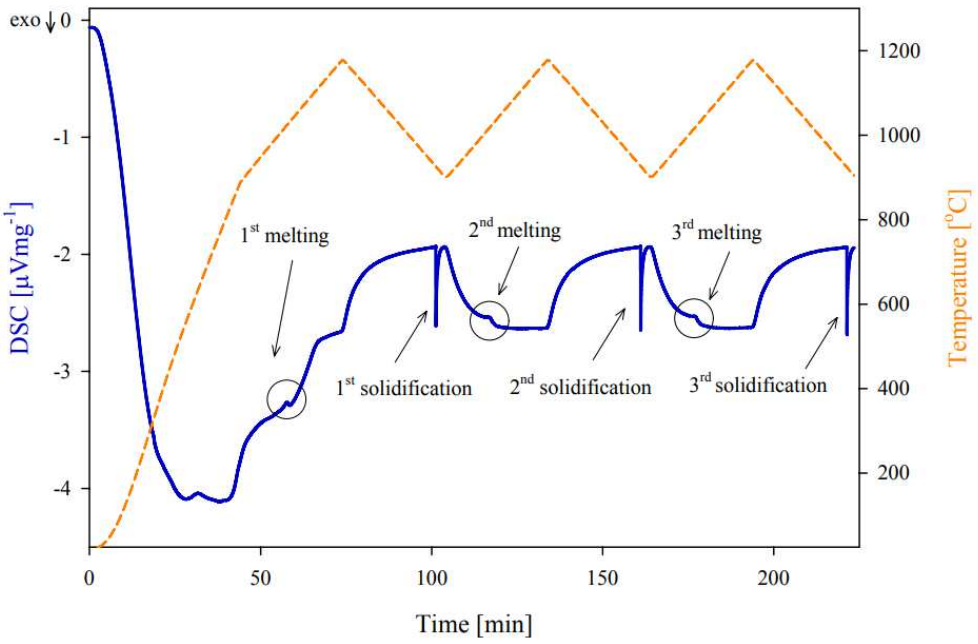

Figure 4.3: ThF_4 DSC curve produced following purification at Ontario Tech University. Copied from Lipkina [12].

Analyzing available literature on actinide purification provides a vague description on used processes, but the effect of certain variable manipulations remains either unexplored, unreported, or unable to draw conclusions from. One such variable is

the ratio of ammonium bifluoride to actinide fluorides, which was explored by Lipkina[12], but it was not reported by others[14,19,36]. Because of the lack of information on this subject, the observed magnitude of impurities experienced by the as-received salts also remains undetermined. Information on reaction kinetics and ramp rate's effect on thoroughness of reaction is scarce, but successful reactions between actinides and ammonium bifluoride ranges from a total of 18 hours to over 40 days [19,36,37]. This range of reaction times, however, is skewed by the use of significantly different temperatures and targeted reactions, so their direct comparison can be misleading.

CHAPTER 5: METHODOLOGY

This chapter describes a designed purification system and its components for use in oxygen minimization and removal and scrubbing of HF gas. The procedures that the system was used for are also described, and experimental techniques used to analyze results are explained for the purpose of replicability.

5.1. Materials

The use of excess ammonium bifluoride within the reaction vessel, which will be heated well above the material's boiling point, guarantees the release of HF gas from the purification process. HF gas is known to attack glass and could potentially present a concern to the glovebox containing the purification system, so a removal system was a necessity for the purposes of this process. The material chosen to react out flowing HF was potassium hydroxide due to its operational history found in literature [14,21,38–40].

Nickel is considered to be the most corrosion-resistant material in the presence of HF (with the exception of Mo which makes a poor structural material) due to the material's highly negative Gibbs energy for the formation of a passive layer of NiF_2 when in contact with fluorides [20,41–43]. For this reason, the reaction vessel discussed in section 5.2 was chosen to be made of nickel.

KOH that was used in the reaction system was sourced from BTC Chemical and has a purity above 85%. Ammonium bifluoride was sourced from Sigma-Aldrich and was said to be 95% pure. Uranium tetrafluoride used for all purification efforts was

sourced from ORNL and was synthesized by high temperature fluorination of uranium metal. At the time of shipping, it was considered to be over 99% pure. Graphite crucibles used were sourced from OTOOLWORLD.

5.2. Reaction System

The reaction vessel purchased for this purification process can be seen in Figure 5.1 below and a 3D rendering of it is shown in Figure 5.2.

Figure 5.1: Shown is the nickel Parr 4740 reaction vessel purchased for purification efforts.

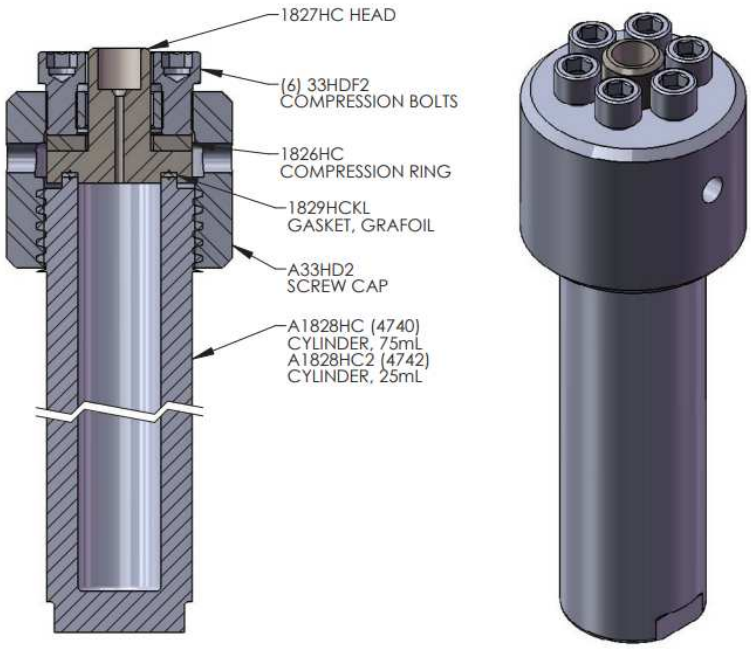

Figure 5.2: 3D rendering of a 4740 type reaction vessel provided by Parr Instruments.

During trials, this vessel is heated by SAMOX heating tape sourced from BriskHeat with temperature capabilities of up to 700˚C connected to an analog interfaced SDC temperature controller with a built in J-type Thermocouple. In Figure 5.3, the vessel with applied heating tape with maximal surface contact ensured using pipe clamps can be seen.

Figure 5.3: Reaction vessel with applied heating tape.

This vessel was modeled after the vessel chosen by Ontario Tech University for their purification work. The main difference between the two vessels is the inclusion of an additional needle valve and port to allow for the flow of purge gas through the vessel. This vessel is rated up to 1000 psi at 250˚C. The head and cylinder portions of the vessel are constructed of Ni 200, as is the gasket used to ensure sealing. The vessel includes a 1000 psi rupture disc made of gold faced Ni alloy 600, and the needle valves are Ni alloy 400.

The reaction vessel faced significant heat loss from the unheated base which exasperated already present thermal lag between the heating tape and the vessel. To combat this, a half inch thick base plate of calcium silicate was placed beneath the vessel.

Along with this base plate, as shown in Figure 5.4, mineral wool piping insulation was placed around the vessel and tied shut using copper wiring during heating. The top of the vessel was insulated using a piece of fiberglass insulation, and a K-type thermocouple was added to the system at a location without heating tape to monitor thermal lag.

Figure 5.4: Parr reaction vessel with mineral wool insulation applied placed on a calcium silicate base plate.

Particularly at the high dwell temperature, uranium compounds possess a high propensity for oxidation. This was evidenced by visual oxidation of initial trials despite being run under argon flow. In an attempt to minimize the amount of oxygen that reached the reaction vessel, several precautions were taken. First, all inlet lines of the system which were originally PTFE were replaced by copper tubing to eliminate the chance of permeation of oxygen through the tubing. In addition to this, a Setnag Gen'Air

was included between the argon cylinder and the glovebox to remove the low levels of oxygen impurity from the cylinder.

A Rapidox 3100 Series oxygen detector was used to determine the oxygen content flowing through the system. Without the use of the Gen'Air, the O_2 levels of the system were measured at 28 ppm. With the addition of the Gen'Air, levels were measured at 10 ppm, and this was further reduced to less than 6 ppm with the application of vacuum grease on the external fittings of the system. These values are likely above the true values due to the use of PTFE tubing between the glovebox and the Rapidox which allows nonzero quantities of oxygen permeation.

For the removal of HF gas, an excess of potassium hydroxide was loaded into three Savillex 60 mL PTFE impingers that were placed in series along the PTFE tubing connected to the outlet of the vessel. The HF gas is pushed through the impingers by the argon being flown through the system when in operation. Following the impinger system, the gas is led outside the glovebox using a custom ¼" bulkhead feed through KF40 fitting and into the lab's snorkel. Figure 5.5 shows a picture of the impinger system and connected tubing, and a full flow chart of the reaction system can be found in Appendix B.

Figure 5.5: Shown is the off-gas system with three in-series PTFE impingers loaded with KOH for the removal of HF gas.

The off-gas being led to the snorkel was checked for HF content using a break tube with a detection range of 1.5-15 ppm of HF gas. The tube showed no indication of HF in the off-gas. The break tube was provided by Ontario Tech University.

Much of this design was adapted from a similar system set up by Dr. Bernie Fitzpatrick out of Ontario Tech University. The use of a flow gas(allowed by the inclusion of a second port in the reaction vessel) was novel to this system, as well as the inclusion of KOH as a scrubber material for flowing HF. The removal of the needle valves to allow constant removal of gaseous by-products was also a distinct difference between the off-gas treatment used in this system and that of Ontario Tech University.

5.3 Purification Procedure

A full SOP of the final purification procedure can be found in Appendix A of this thesis. This section will be concentrated on the evolution of this process and the changes

that were undergone to optimize the process in the interest of transparency as well as to address potential problems others undergoing this process may experience.

Prior to purification trials, the OTOOLWORLD graphite crucible is baked for several hours at 500˚C in the glovebox to remove impurities that could potentially be released during a purification trial. Within the vessel, the graphite crucible was placed on a 1.5 inch tall stage to minimize heat loss from the crucible to the unheated base of the vessel.

Figure 5.6: Graphite crucible with lid with a diameter of 20 mm used to hold powder samples.

Graphite is considered non-reactive in the presence of HF, and therefore was considered to be a suitable material [18,44]. However, with the graphite crucible, potential interaction is a possibility between HF and any silica impurities in the crucible of this thesis. However, it is unlikely that this reaction will occur at more than a minimal capacity due to water's necessity for it to proceed [45,46]. The products created by this reaction are gaseous in nature, so they would not be considered problematic for the

purification process regardless. This could, however, result in sample mass being slightly lower than expected following the purification procedure.

Initial trials with just ammonium bifluoride were run under a fume hood for 4 hours at 180˚C before a ramp to 400˚C for 1 hour. Calculations to determine sample size were conducted using the ideal gas law to ensure pressures remained below the vessel's limit.

A very large amount of interaction between the HF and the vessel was observed (seen in Figure 5.7), and the product was identified as NiF_2.

Figure 5.7: Shown are the results of a trial run with just ammonium bifluoride.

While the crucible in use was covered, it was not threaded and there was still a high likelihood of NiF_2 contamination in the sample. Furthermore, the reaction vessel's nickel needle valves, which were opened following the low dwell period to allow the vessel to be purged with Ar, were found to clog in these initial trials. This trapped HF gas in the vessel (a safety hazard) as well as the presumed water vapor created during fluorination of any oxides (a purity hazard).

Further trials targeted the solid-solid interaction seen between ammonium bifluoride and uranium tetrafluoride from multiple literature sources [27,32,36,37,47]. These were performed under continuous Ar flow of .1-.5 lpm. Initially, the ratio of ammonium bifluoride to uranium tetrafluoride was set at 2:1, the low dwell period was 125˚C for 5 hours, the high dwell period was set at 440˚C for 4 hours, and the ramp rate was 10˚C/min. The trial lengths were varied in subsequent trials and Mixing of the ammonium bifluoride and uranium tetrafluoride was performed under Ar within a glovebox using a mortar and pestle for a minimum of 15 min (shown in Figure 5.8).

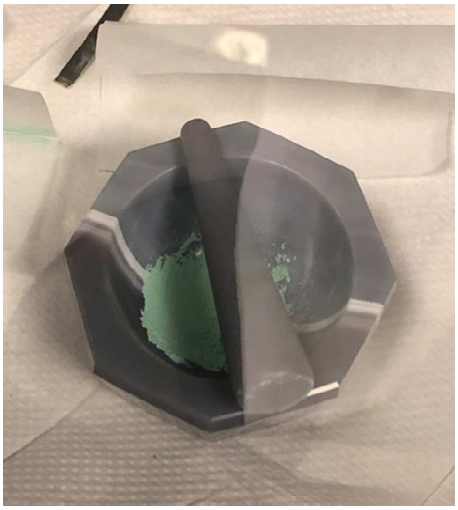

Figure 5.8: The mortar and pestle used under Ar with the ammonium bifluoride and uranium tetrafluoride mixture.

Trial procedures developed based on observed results. In the pursuit of process optimization, different variables were explored. Significant trial procedures adopted during the process's evolution that resulted in quantifiable partial success or furthered understanding of the reaction are listed in Table 5.1.

Table 5.1: Purification Trial Procedures

Trial Procedure Number	Low dwell temperature and duration	High dwell temperature and duration	Target Powder Ratio (NH_4HF_2:UF_4)	NH_4HF_2 in mixture	UF_4 in mixture	Ramp Rate
1	125˚C for 5 hours	440˚C for 4 hours	2:1	367.4 mg	191.8 mg	10˚C/min
2	110˚C for 5 hours	440˚C for 4 hours	1:1	175.4 mg	168.0 mg	10˚C/min
3	110˚C for 6 hours	480˚C for 4 hours	1:1	409.8 mg	394.8 mg	5˚C/min
4	100˚C for 6 hours	480˚C for 6 hours	1:2	131.3 mg	261.8 mg	3˚C/min
5	100˚C for 7 hours	480˚C for 8 hours	1:2	98.5 mg	194.4 mg	3˚C/min
6	100˚C for 7 hours	480˚C for 16 hours	1:2	95.7 mg	188.7 mg	3˚C/min
7	100˚C for 14 hours	480˚C for 8 hours	1:2	90.2 mg	178.1 mg	3˚C/min

5.4. Analysis

All preparation of DSC samples was performed in a glovebox in an Ar environment.

DSC sample crucibles consist of a stainless steel base with threads to connect to a stainless steel top, a nickel liner, and a nickel gasket (shown in Figure 5.9).

Figure 5.9: DSC crucible top, base, liner, and gasket from left to right.

The process began by placing a liner inside the crucible base on a Netzsch sealing press. This base with the liner was then placed in a plastic weighing boat and weighed on a VWR B2-series precision scale prior to being loaded with a sample mass of 10-30 mg. Once the sample was loaded using a fixed plastic funnel, a nickel gasket was placed on top of the base. The screw-on crucible top was applied using an adjustable torque wrench set to 3.0 Nm to the base placed on the Netzsch seal press. This ensured the crucible would be sealed in a leak-tight manner.

Once this crucible was sealed, it could be removed from the glovebox and loaded onto the Netzsch STA 409 CD device. The sample carrier contains one reference crucible and one sample crucible when run and incorporates the use of a Zr ring as a method of oxygen removal. Due to a learning curve regarding uranium materials' rate dependence on melting point, heating rates for DSC runs initially varied. Later measurements were performed at a rate of 10 K/min under 70 ml/min Ar. The trials run were taken from room temperature to either 1150˚C or 1200˚C then cooled to 700˚C or 800˚C, depending on the trial, then returned to the top temperature and cooled to the lower bound again. A visualization of this heating pattern can be found in Figure 5.10.

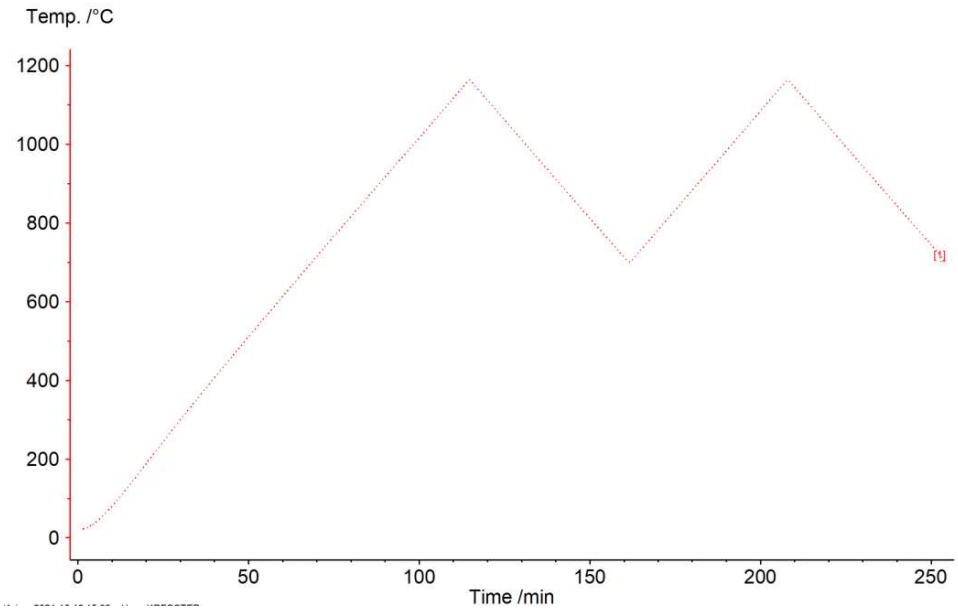

Figure 5.10: Temperature Curve used during DSC trials.

XRD analysis was conducted using a Rigaku Smartlab X-ray Diffractometer at room temperature in transition mode over 15 min. Samples were prepared in within an Ar filled glovebox, and due to the high absorption of uranium, thin-walled quartz capillaries with .3 mm outer diameters and a wall thickness of .01 mm had to be used to contain the samples. Due to the brittleness of the capillaries, they were placed inside a sturdier pyrex capillary to be handled. The thin-walled quartz capillaries were loaded using a packing fraction of approximately .1 by carefully placing powder in the cone portion of the capillary, shown in Figure 5.11, and rubbing a file against the exterior to allow the powder to fall. The capillaries were sealed using clay to keep the salt from reacting with the environment upon being removed from the glovebox.

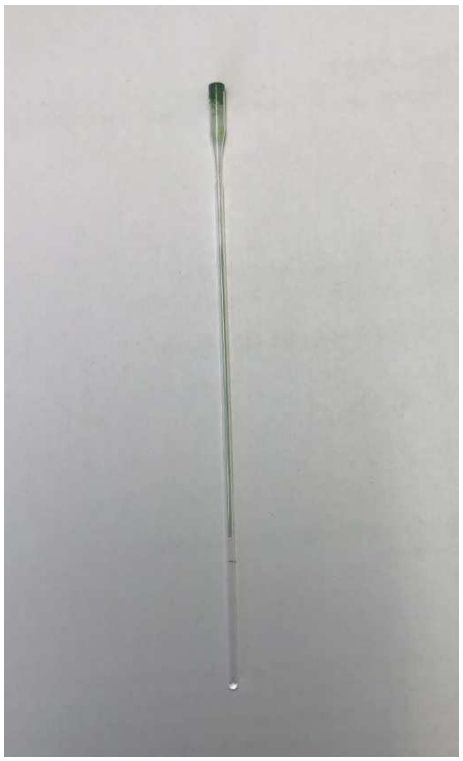

Figure 5.11: .3 mm outer diameter quartz capillary used to hold the salt during XRD analysis.

For the ICP-OES analysis, samples between 5 and 10 mg were loaded into a 75 mL PTFE vessel along with 8 mL of aqua regia (created using a 8:4:3 ratio of HNO_3:HCL:H_2O). The vessel then underwent digesting using a Perkin Elmer Titan MPS set to a 10 minute isothermic hold at a temperature and pressure of 175˚C and 30 bar with heating from room temperature being conducted at a rate of 5˚C/min. This heating cycle was followed by a cooling cycle to 50˚C at a rate of 1˚C/min.

Following digesting, the concentration of the sample had to be diluted to bring the final sample concentration within the measured range of the Perkin Elmer Avio 200 ICP-OES machine (1-10 ppm). This was done by taking .1 mL of the digested mixture from the vessel and loading it into a plastic sample container and diluting it with 9.9 mL of water. All loading of liquids for the ICP-OES procedure was done using a VWR pipettor

to ensure precision. Calibration was conducted using calibrant liquids with known concentrations of aluminum, calcium, iron, magnesium, nickel, and strontium. All calibration data can be found in Appendix C1 of this thesis. The software used to manage the data was Syngistix for ICP by Perkin Elmer.

CHAPTER 6: RESULTS

Many iterations of purification trials were run, as outlined in Table 5.1, to establish an optimal purification method and to understand the effects of various parameters (in particular, the dwell periods). Trial results were assessed visually and by weight initially. All trials resulted in a solid puck of material located at the center of the graphite crucible that could be broken into finer powders, and all provided weights have the initial weight of the crucible subtracted from them. Theoretical masses are calculated using the total material in the full crucible prior to heating multiplied by the proportion UF_4 in the mixed powders (a small amount is lost in the mixing process). For theoretical mass calculations, an arbitrary 1% of UO_2 impurity is assumed based on the greater than 99% purity claimed, and theoretical masses indicate full fluorination of this impurity. Trials that possessed a puck which appeared uniform in color, and thus possible purity, had their melting points measured by DSC. In the temperature range of the UF_4 melting point, we ran sodium fluoride (melting point of 995.9˚C) in the same conditions (heating rate of 10 K/min), and the measured melting point was shown at 990.5˚C, meaning that a correction factor of approximately 5˚C to the upside is reasonable for observed measurements. The resulting data from these assessments is presented in this chapter.

The initial weight, theoretical final weight, and observed final weight of each method compared to theoretical values is shown in Table 6.1 along with the analysis methods of each individual trial product.

Table 6.1: Trial Results and Analysis Methods

Procedure Number	Initial Weight	Theoretical Final Weight	Observed Final Weight	Forms of Analysis Conducted
1	554.4 mg	191.8 mg	177.2 mg	Visual
2	340.8 mg	168.3 mg	172.5 mg	Visual, DSC
3	781.6 mg	387.9 mg	406.2 mg	Visual, DSC
4	387.5 mg	261.07 mg	246.5 mg	Visual, DSC
5	292.5 mg	196.7 mg	187.9 mg	Visual, DSC, ICP-OES, XRD
6	284.4 mg	190.9 mg	185.7 mg	Visual, DSC
7	268.3 mg	180.1 mg	176.8 mg	Visual, DSC

6.1. Trial Procedure 1

Trial procedure 1 from Table 5.1 consisted of a low dwell period of 5 hours at 125˚C, a high dwell period of 4 hours at 440˚C, approximately a 2:1 mass ratio of NH_4HF_2 to UF_4, and a ramp rate of 10˚C/min. The outcome, shown in Figure 6.1, possessed a metallic grey layer that appeared to have been melted near the edges of the crucible and a black solid layer around the edges of the puck. Central portions of the puck did possess a green color as shown.

Figure 6.1: Final product of trial procedure 1 showing large amounts of oxidation and a grey layer around edges of the crucible.

6.2. Trial Procedure 2

Trial procedure 2 from Table 5.1 consisted of a low dwell period of 5 hours at 110˚C, a high dwell period of 4 hours at 440˚C, a 1:1 powder ratio, and a ramp rate of 10˚C/min. The outcome of this trial was a uniform green puck with no visual impurities. The final mass of the crucible was high compared to the theoretical mass as shown in Table 6.1. A DSC curve of the final product run at a rate of 20 K/min is shown on initial heating in figure 6.2 and in full with varied heating rates in figure 6.3. The initial heating curve possesses a peak at 1039.1˚C with an onset temperature of 1020˚C. On cooling, a sharp peak occurred at 790˚C.

The exact procedure used to achieve these results was followed two more times, and results were not found to be replicable.

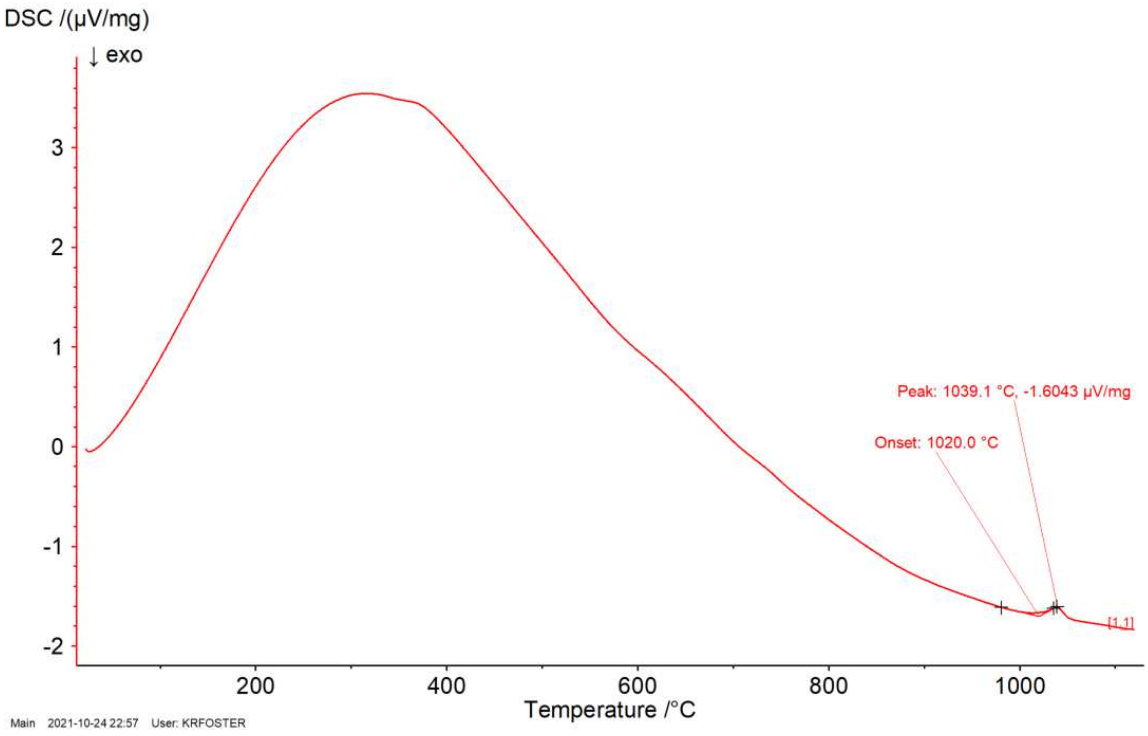

Figure 6.2: Initial heating curve at 20 K/min of UF_4 purified by purification procedure 2.

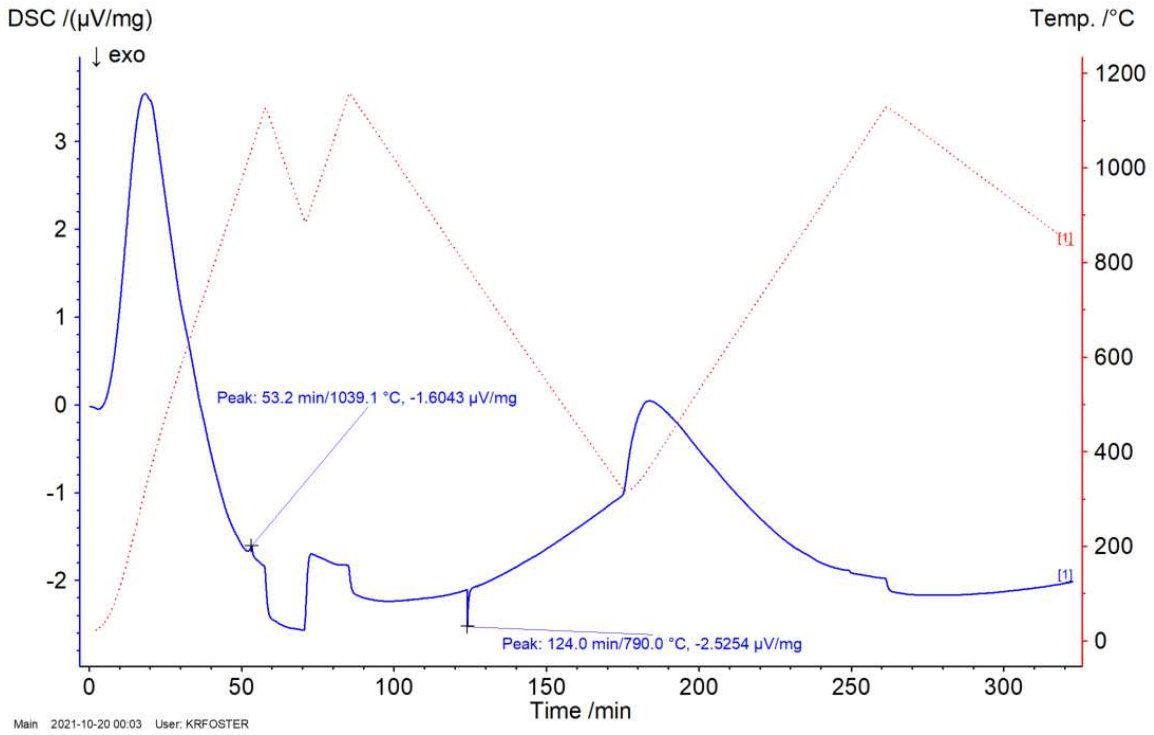

Figure 6.3: Full DSC curve of UF_4 purified by trial procedure 2 with varied heating rates (20 K/min followed by 10 K/min).

6.3. Trial Procedure 3

Trial procedure 3 from Table 5.1 consisted of a low dwell period of 6 hours at 110˚C, a high dwell period of 4 hours at 480˚C, a 1:1 powder ratio, and a ramp rate of 5˚C/min. The top layer of the reaction product was a metallic gray, but beneath this exterior was a uniform green powder. Regrettably, a picture was not taken before the grey exterior was broken, however, Figure 6.4 shows a portion of this grey layer along with the powder found beneath it. Based on the observed green powder, a DSC measurement was run on the powder product at a rate of 2 K/min, as shown in Figure 6.5.

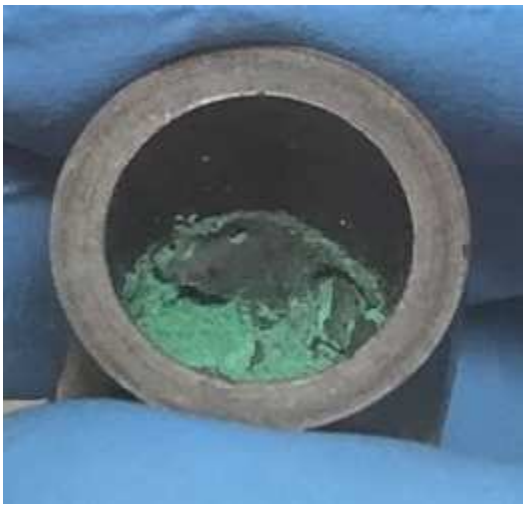

Figure 6.4: Crucible content following trial procedure 3.

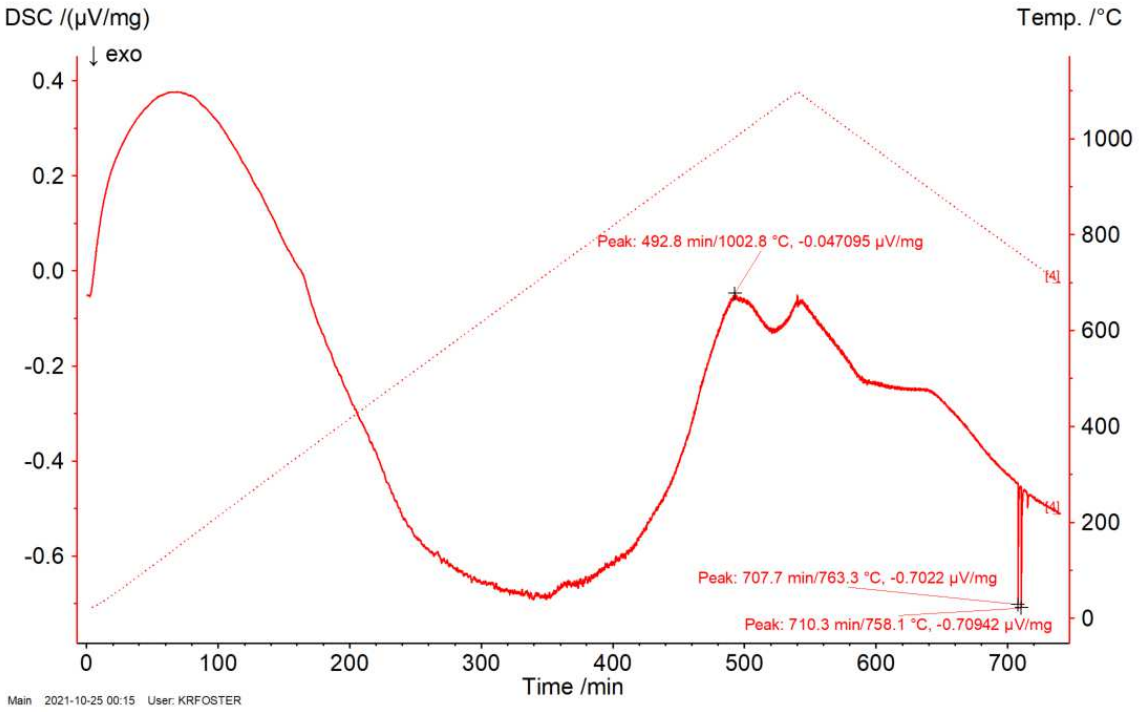

Figure 6.5: DSC curve of the powder produced using trial procedure 3 heated at 2 K/min.

6.4. Trial Procedure 4

Trial procedure 4 from Table 5.1 consisted of a low dwell period of 6 hours at 100˚C, a high dwell period of 6 hours at 480˚C, a 1:2 powder ratio, and a ramp rate of

3˚C/min. Visually, the product looked to be a uniform green powder with slight grey shading around contact points with the graphite crucible, as shown in Figure 6.6. A DSC curve of the trial was taken at 10 K/min and is shown by Figure 6.7. Initial heating showed a peak at 1021.6˚C, and cooling data showed a consistent peak around 750˚C.

Figure 6.6: Uniform green puck resulting from purification using trial procedure 4.

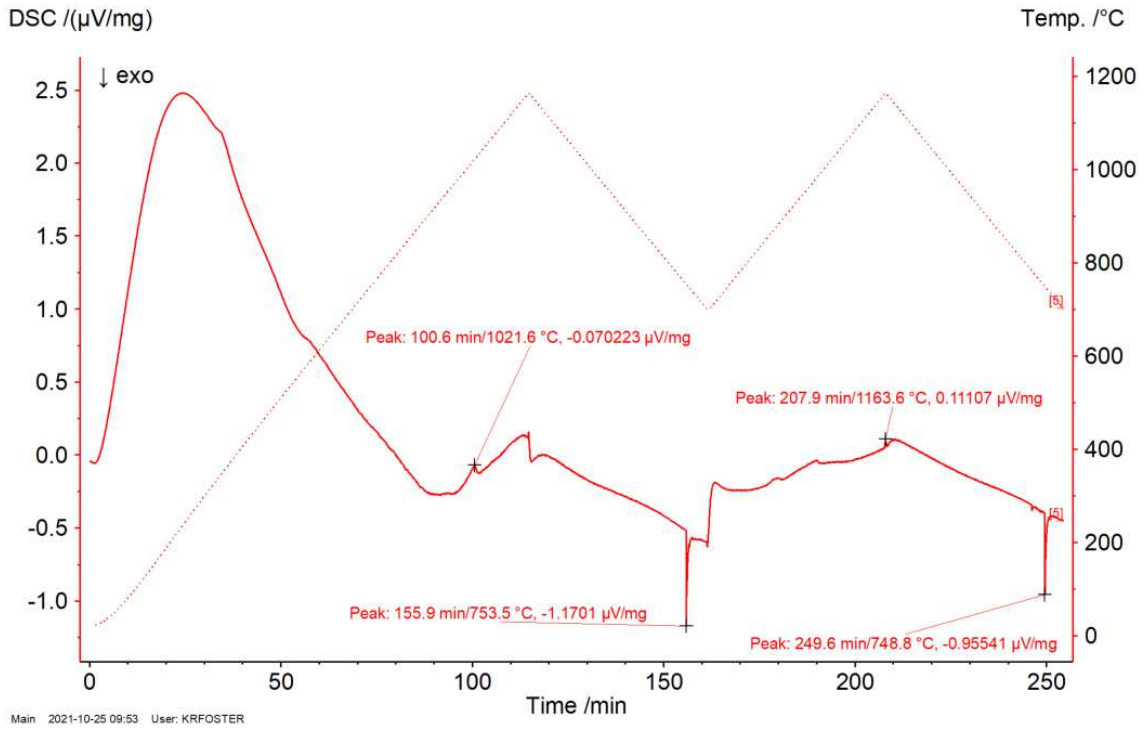

Figure 6.7: DSC results of trial procedure 4 at a heating rate of 10 K/min.

6.5. Trial Procedure 5

Trial procedure 5 from Table 5.1 consisted of a low dwell period of 7 hours at 100˚C, a high dwell period of 8 hours at 480˚C, a 1:2 powder ratio, and a ramp rate of 3˚C/min. The resulting powder was a uniform green puck with no visual impurities very much like that shown in Figure 6.7. A DSC measurement to determine the sample's melting point was run on this trial at a heating rate of 10 K/min, and the results are found in Figure 6.8. On initial heating, a peak was identified at 1032.7˚C with an onset of 1020.9˚C. On cooling, peaks were identified at 778.8˚C and 769.1˚C.

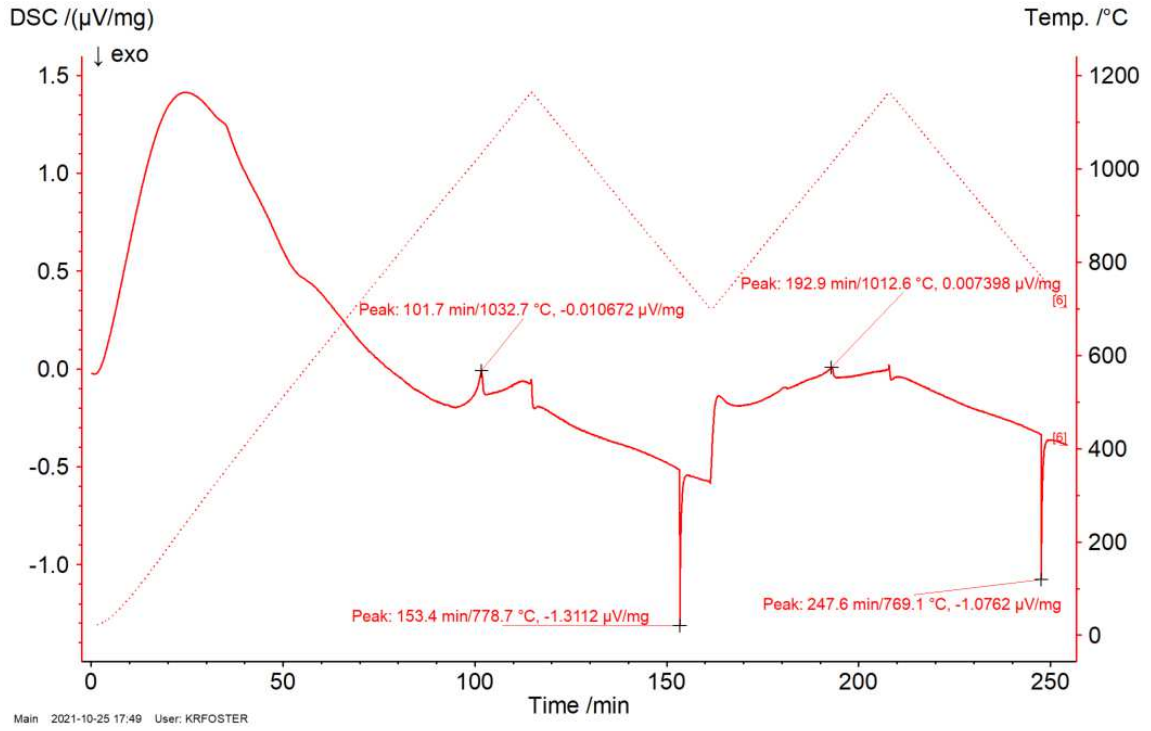

Figure 6.8: DSC results of trial procedure 5 at a heating rate of 10 K/min.

Analysis of the salt using ICP-OES was conducted and the full data from this as well as the calibration curves can be found in Appendix C of this work. The produced salt and the original ORNL salt were checked for aluminum, calcium, iron, uranium, magnesium, nickel, and strontium content, and the findings are shown in Table 6.2.

Table 6.2: ICP-OES Concentrations in Calibration Units for UF_4 Samples

Sample	Ca (mg/L)	Al (mg/L)	Fe (mg/L)	U (mg/L)	Mg (mg/L)	Ni (mg/L)	Sr (mg/L)
Trial Procedure 5 UF_4	0.273	-0.011	0,007	5.130	0.007	0.002	0.000
ORNL As-received UF_4	0.226	-0.012	0.003	4.757	0.006	.001	0.000

Further analysis was performed on this purified sample and the as-received UF_4 using XRD. The results of the XRD analysis is shown in Figure 6.9. In this figure, the red points show data from this XRD run, the black lines show the expected peaks modeled using the Rietveld refinement method, and the blue lines show the variation between the two. Vertical lines in the figure show where peaks are expected.

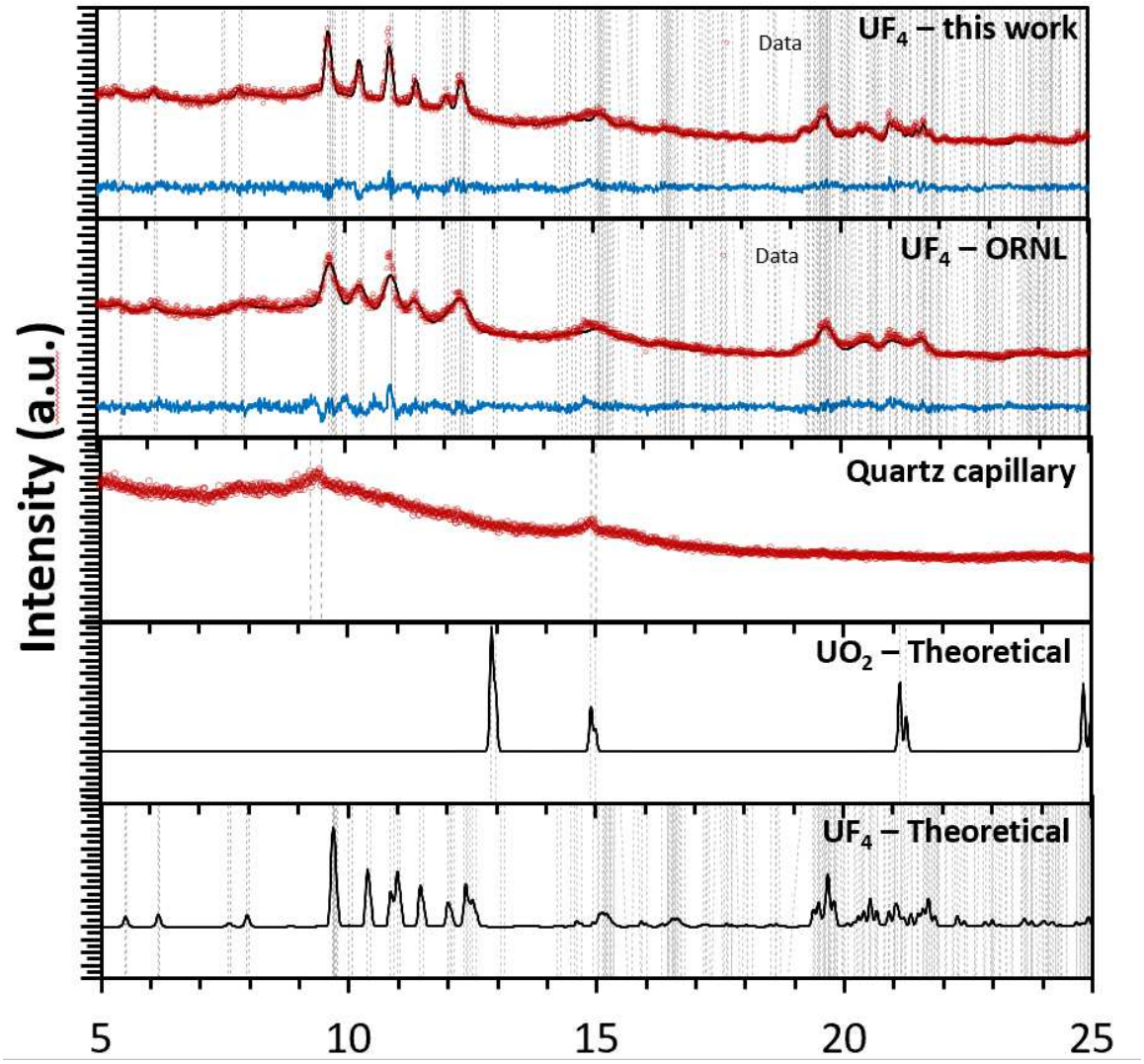

Figure 6.9: Results of XRD analysis run on salt that underwent purification using trial procedure 5 and as-received salt from ORNL.

6.6. Trial Procedure 6

Trial procedure 6 from Table 5.1 consisted of a low dwell period of 7 hours at 100˚C, a high dwell period of 16 hours at 480˚C, a 1:2 powder ratio, and a ramp rate of 3˚C/min. The result was a green puck that matched the previous two trials with no apparent visual impurities. DSC was run on this sample at a heating rate of 10 K/min, and the results are found in Figure 6.10. On initial heating, the DSC curve showed an

onset of 1023.5˚C and a peak of 1032.2˚C. On cooling, the curve showed a peak at 769.2˚C.

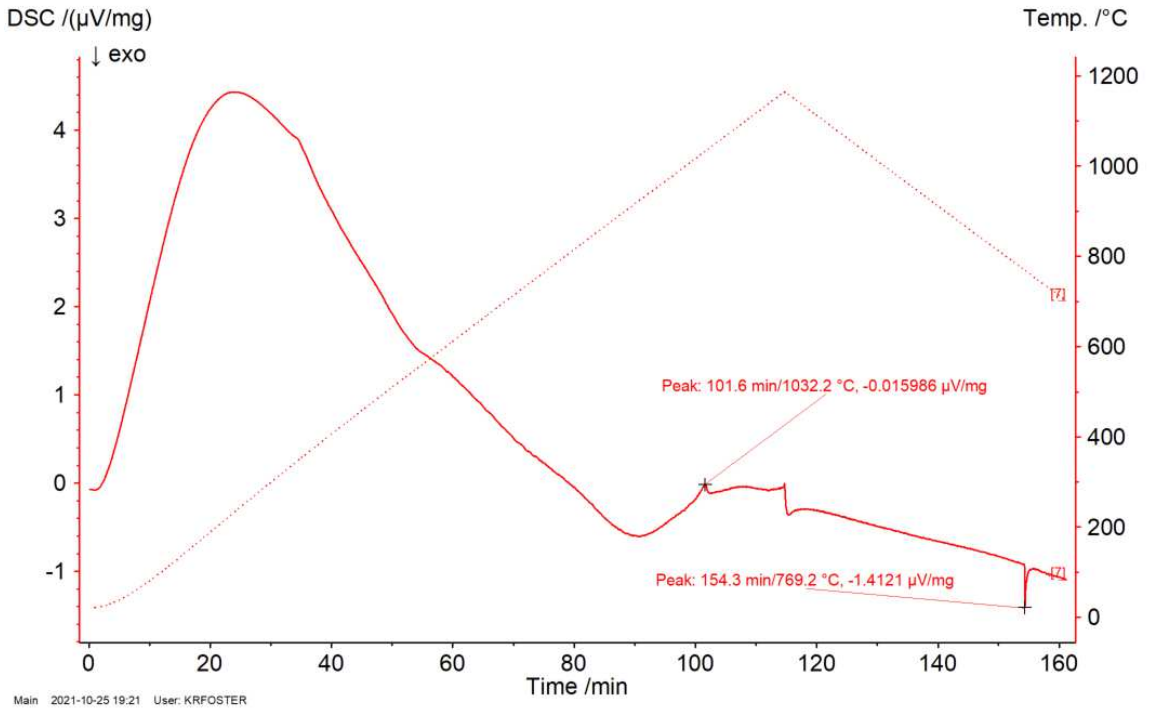

Figure 6.10: DSC results of trial procedure 6 at a rate of 10 K/min.

6.7. Trial Procedure 7

Trial procedure 7 from Table 5.1 consisted of a low dwell period of 14 hours at 100˚C, a high dwell period of 8 hours at 480˚C, a 1:2 powder ratio, and a ramp rate of 3˚C/min. The resulting powder possessed two small black spots on top of the puck as shown in figure 6.11, but otherwise, the powder appeared to be consistent in color and form with expectations of UF_4. The melting point of the material was measured by DSC, and the result is shown in Figure 6.12. The DSC curve showed a peak on heating at 1029.5˚C with an onset of 1021.2˚C, and on cooling the peak was found at 756.2˚C.

Figure 6.11: Result of trial procedure 7 with presence of black spots in product.

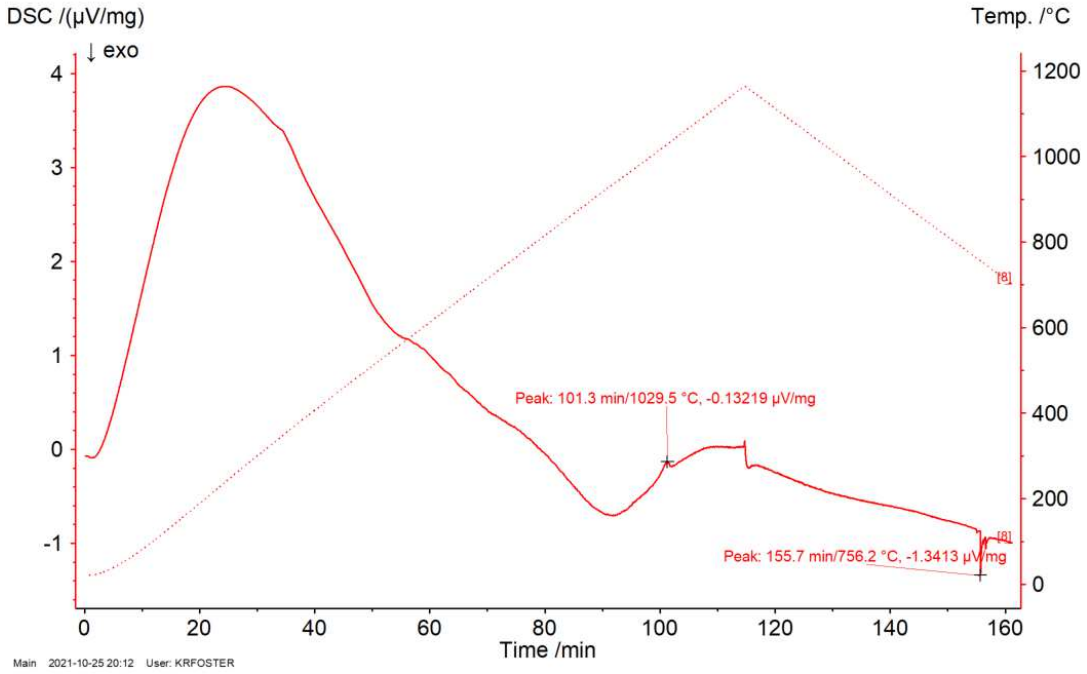

Figure 6.12: DSC results of trial procedure 7 at a rate of 10 K/min.

6.8. General Comparisons

A comparison of the DSC curves from initial heating for the as-received UF_4 and trial procedures 5-7 is shown in Figure 6.13, and a direct comparison of trial 5 and as-received UF_4 is shown in Figure 6.14.

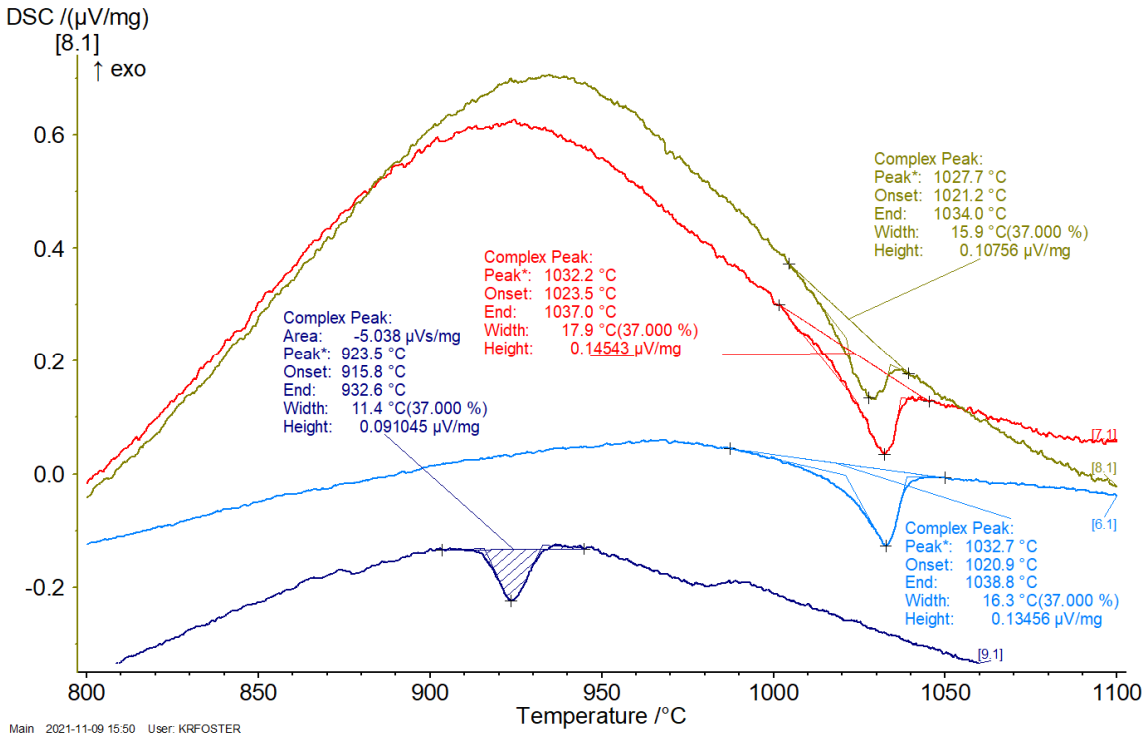

Figure 6.13: Comparison of as-received UF_4 to UF_4 that underwent purification. The curve labeled 6.1 (blue) shows procedure 5, 7.1 (red) shows procedure 6, 8.1 (green) shows procedure 7, and 9.1 (purple) shows as-received UF_4 from ORNL.

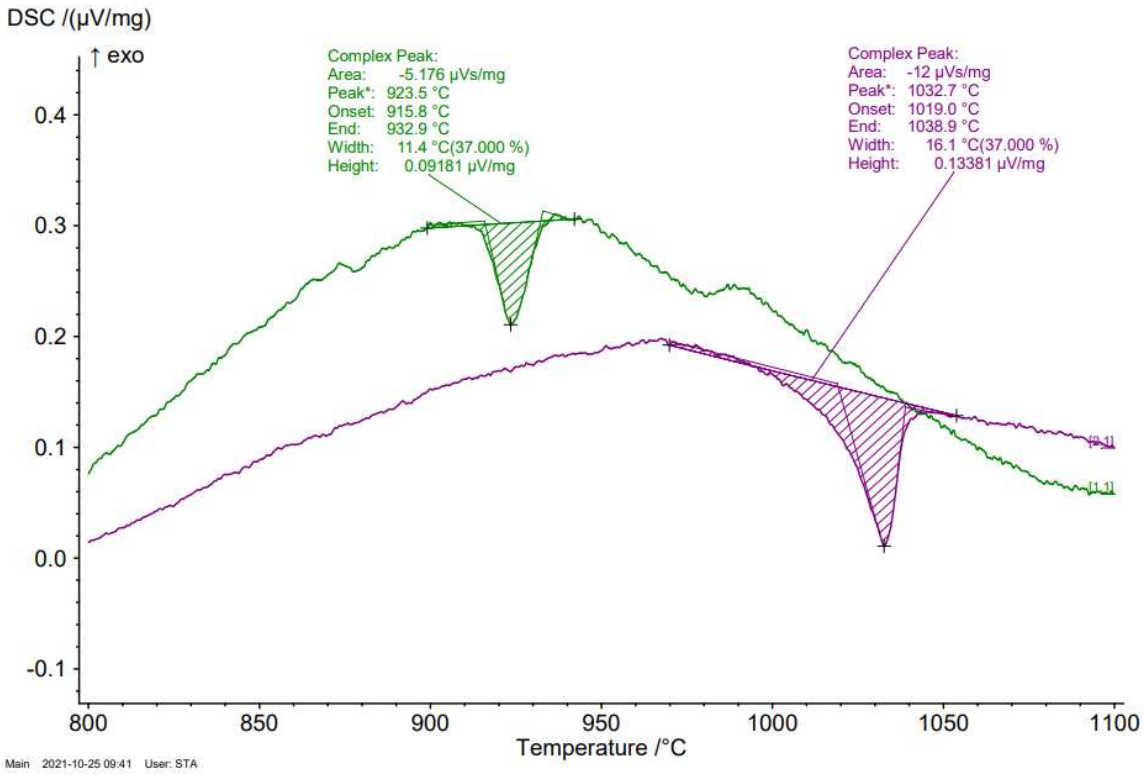

Figure 6.14: DSC curves in the range of 800˚C to 1100˚C for product from trial procedure 5 (purple) and as-received UF_4 (green).

CHAPTER 7: DISCUSSION

The procedures shown in Table 5.1 were developed over time based on current understandings of the reaction between ammonium bifluoride and uranium tetrafluoride. This chapter will discuss the goals of each trial and what was learned from them. This work will also be compared to existing literature and theories will be provided regarding the material behavior based on results seen.

It should be noted that while weighing of the final samples provided some knowledge regarding final product composition, all samples deviated from the calculated theoretical final weight to the low side between 3 to 10% with the exception of procedure trial 3. When analyzed using DSC, these products with low observed final weights still possessed melting points much more consistent with literature values of 1034.7˚C to 1036˚C. As such, observed final weights were not considered to be good indicators of purity. Differences in mixing composition added to the mortar and pestle versus that of the powder that makes it in the crucible (a small amount is lost to the mortar and pestle) present one possible reason for this. Further, the mass of the uranium molecule in both uranium dioxide and uranium tetrafluoride provides the bulk of the molar mass of these compounds, with the total mass being diluted even more due to the 6-7 g graphite crucibles, so the margin of error is likely higher than ideal on these measurements. As discussed in section 5.2 of this thesis, possible interaction between resulting HF and silica impurities of the graphite crucible could be another possible explanation for the discrepancy of theoretical final weight versus observed [44,45]. These factors lead to DSC,

XRD, and ICP-OES being preferred analysis methods to draw conclusions from within this work.

In all trials that presented a proper heating point on DSC on initial heating, subsequent heating beyond the melting point did not present the same peak, and more often than not, no peak was experienced at all. On cooling, a sharp peak appears at the mid to high 700s, but not at the initial melting point, for every cooling curve. The most apparent explanation is an overcooling (an overly stable liquid state) followed by a loss of the long range ordering of the salt.

From the 1980s, Fedorov out of the Shubnikov Institute of Crystallography describes U^{4+} as a 2nd degree glass former based on structural, physicochemical, and energetic properties of the compound and their relationship with the cation's coordination number[48]. A 2nd degree glass former is a material that can form a glass in the presence of just one other modifier. In the case of the observed behavior, it is possible that the presence of uranium oxide could be acting as this modifier leading to glass-like behavior. More light could be shed on this subject by the use of high temperature XRD analysis of the purified sample.

7.1. Trial Procedures 1-4

Trial procedures 1-4 are grouped together as this period represented a steep learning curve faced in this work. While only one final product with significant oxidation is shown, this procedure and outcome was seen several times due to system complications. As discussed in section 5.2, this led to the addition of some key oxygen removal components that made all the work done since possible. However, final

products for the trials within this range were viewed skeptically due to concerns with the system oxygen content.

The use of a 2 to 1 ratio of ammonium bifluoride to uranium tetrafluoride in initial trials was due to the claim that higher molar ratios of ammonium bifluoride would still lead to the formation of actinide tetrafluorides at high temperatures (400-425˚C for uranium) [24,27]. This claim was not disproven in this work due to differences between systems being used to purify actinide oxides, but large amounts of what was assumed to be residual ammonium bifluoride (metallic grey portion of the final product) still remained present in the crucible following completion of the trials. This is likely due to the addition of a lid to the crucible to keep the powder inside separated from possible NiF_2 formation which could lead to purity concerns like the ones described by Claux et al[21]. While the lid was not screwed on the crucible, this would present a barrier in the speed with which gaseous products would be removed from the interior of the crucible, which seemed to require longer high dwell periods (evidenced by Figures 6.1 and 6.4). Alternatively, this residual ammonium bifluoride, which was hypothesized to have been seen in trials 1 (2:1 ammonium bifluoride to uranium tetrafluoride) and 3 (1:1 ammonium bifluoride to uranium tetrafluoride), could have been removed with open vessel heating as described by works out of Ontario Tech University and TU Delft [11,12,19]. Due to concerns with oxidation and, primarily, the releasing of HF into the glovebox, this method was not employed in this work. While trial procedure 2 was found to be successful in improving melting point behavior by DSC at a ratio of 1:1 ammonium bifluoride, the results could not be replicated with the same parameters. Trial procedure

4 begins the use of a 1:2 ratio of ammonium bifluoride to uranium tetrafluoride, for which ammonium bifluoride was seen to be consistently reacted off completely.

The changes in low dwell period from trial procedure 1 to trial procedure 2 and 3 to trial procedure 4 is a result of overshooting of the heating tape that was observed by the J-type thermocouple attached to the heating tape's temperature controller. The heating tape continually turns on and off based on the readings of the thermocouple, and when the tape is on, it was observed to overshoot low temperatures by up 30˚C. This jump in temperatures would risk melting the ammonium bifluoride, so the low temperatures were adjusted accordingly. The low dwell duration was based on the work of Yeamans[27], where he claimed at 110˚C, fluorination proceeded in full in 2.5 hours, but this was following slight manual agitation over 17 days between UO_2 and UF_4. This low dwell period was increased to 6 hours to account for this difference.

The gradual decrease in ramp rate was added to combat the reformation of oxygen impurities that were believed to be present to a small degree in final products much like the one shown in Figure 6.11. It was believed this would allow less oxygen interaction with the salt in the range where the formation of UO_2F_2 is favored (T>250˚C) [31]. Results of trial 3 and 4 were improved following this change (when compared to replication attempts based on trial procedure 2), but more work would need to be done with varied ramp rates to be conclusive on the topic.

The increase in high dwell temperature between trials 2 and 3 follow changes in the insulation of the system to a slightly less porous material. The addition of a K-type thermocouple to the system to be placed at a location without heating tape revealed thermal lag at the high end temperatures by up to 50˚C. The reaction process described

by Yeamans[29] and Benz[38] would indicate that this lag would lead to different final products besides UF_4. The work of Yahata et al. [33] and Pomiro et al.[31] described the stability of UF_4 at temperatures up to 580˚C, so it was considered safe to increase the high dwell temperature to 480˚C to account for thermal lag.

The DSC measurements of trial procedures 2 and 3 revealed the sensitivity of uranium salts to heating rates. While trial procedure 2 (Figure 6.3) looked very consistent with literature values with a strong peak 1039.1˚C, trial procedure 3 showed significant wavering in the range of 600-800˚C. This led to the selection of a uniform heating rate of 10 K/min based on the work of Soucek et al. [15] which would allow comparison to literature data and future data.

7.2. Trial Procedures 5-7

Trial procedures 5-7 represent trials that are much easier to directly compare the results of due to the development of an established and consistent process with regards to heating rate, powder ratios, and trial temperatures as shown in Figure 6.13. These trials were used to determine the effect of varied dwell periods at high and low temperatures. Trial procedure 5 was used as the baseline for comparison between procedures 6 and 7 which doubled the high temperature period duration and the low temperature period duration, respectively.

When compared to trial procedure 5, trial procedure 6 (with a 16 hour high dwell period) had a very comparable peak temperature with the difference between the two only being .5˚C. This temperature is very consistent with literature values of 1036˚C [29] when the correction factor of ~5˚C discussed in the introduction of chapter 6 is added. The onset temperature is typically the value used in literature to determine the melting

point of a material, however [1,12,15]. The onset temperature of trial procedure 6 is improved by a full 4.1˚C compared to trial procedure 5, and this is consistent between trial procedures 5 and 4, as well. While more trials would be beneficial to determine consistency of these results, longer higher dwell periods seem to improve the depth of DSC peaks and the onset temperatures on melting.

When comparing DSC results of trial procedure 5 and 7, Figure 6.13 shows little to no improvement as a result of a longer high dwell period. In fact, both the onset temperature and the peak temperature of trial procedure 7 (1015.9˚C and 1027.7˚C) show slightly worse results when compared to literature values than that of trial procedure 5 (1018.9˚C and 1027.7˚C) [15]. While more iterations of these trials would need to be run to draw full conclusions, no apparent improvement is evident from increased low dwell periods. The need for further work is particularly true due to the black spots shown in the final product of trial procedure 7. This, believed to be, oxidation was unique to this trial and could skew the results. It is possible this was an anomaly, but further investigation is needed. However, the conclusion on low dwell period is consistent with the conclusion made by Yeamans[27] that as long as sufficient time is allowed for full fluorination (around 2.5 hours after 17 days of room temperature reaction), further low dwell duration provides no benefit.

Each of the trial procedures resulted in an improvement of over 100˚C versus the as-received melting point and onset temperature based on the literature value of 1036˚C [31]. This is a strong indication of improved purity as a result of the purification procedures conducted on the as-received salt.

7.3. ICP-OES and XRD

ICP-OES was conducted on the resulting powder from trial procedure 5, as well as as-received UF_4. The conducting of this analysis was to explore the possibility of a calcium cation impurity of UF_4 put forth by Dworkin[30] out of ORNL with regards to the transition identified for UF_4 at 840˚C by Khripin[13], described in section 4.1.

While undercooling experienced on cooling curves is a well-established common problem in experimental measurements on molten salts, this typically results in errors in measurements of approximately 30-40˚C. This propensity for undercooling possessed by molten salts could explain the lack of available literature on the cooling behavior experienced by UF_4. If such undercooling is being experienced in this work, the observed peaks on cooling show relative agreement with the phase transition that was identified by Khripin et al. within their UF_4 system[13].

The results of the ICP-OES showed a lack of an appreciable quantity of aluminum, iron, magnesium, nickel, and strontium and confirmed the presence of uranium, but it also did show the presence of calcium in a small quantity. The calcium levels observed were seen at a quantity of .226 mg/L in the as-received UF_4 and .273 mg/L in the UF_4 resulting from trial procedure 5. The increase in the as-received quantity to the purified quantity is attributable to different solution concentrations. The acids used to make the used aqua regia to dissolve the powders were tested for calcium content following the results of the UF_4, and quantities were found as shown in appendix C2, but they were of slightly less concentration than the salts. As such, the presence of calcium causing the cooling peak could not be disproven by this analysis.

The XRD of the purified and as-received salts showed only the presence of peaks consistent with UF_4 for both samples. No peaks of UO_2 were revealed with the exception of a small one near 15˚ 2θ value, but this peak is also shown by the quartz capillary that the material was confined in. Data from the XRD shows that the purified UF_4 created by trial procedure 5 shows much sharper and narrower peaks than as received salts, indicating improved crystallinity following the purification process. This improvement on crystallinity could be partially responsible for the improvements seen on the melting point by DSC [49]. An isothermic hold in a furnace or within a DSC machine at greater than 75% of the salt's melting point over a long period before melting could be useful to determine the role of crystallinity on the melting point behavior of the purified salt [50].

CHAPTER 8: CONCLUSIONS

The experimental work on UF4 purification described in this thesis was conducted to fill gaps in knowledge on and to consolidate information regarding actinide fluoride purification without the use of an HF line to encourage future experimental work with the compound. The as-received salt showed evidence of impurities through DSC measurement of its melting point at 923.5˚C compared to the literature value of 1036˚C. The most likely impurities were suggested to be UO2 and UO2F2, and a purification process targeting the solid-state reaction between ammonium bifluoride and the as-received uranium tetrafluoride was designed to remove these impurities.

In details on the process, the initial low dwell temperature was found to be fairly inconsequential so long as sufficient time was allowed for the solid state reaction to proceed to completion. For low dwell duration, results of DSC measurements indicated that six hours provided ample to for the reaction to occur at temperatures above 100˚C, but a precautionary dwell period of seven hours was incorporated to ensure ample reaction time for larger sample sizes. While conclusions can be drawn regarding the high dwell temperature necessity for the particular setup described in this work, the findings may not directly apply to other systems with different components. Exact internal temperatures remain unknown, but a top temperature setting of 480˚C was found to allow the reaction to proceed fully. The duration of the high temperature dwell was found to directly correlate with the observed completeness of reaction, and therefore purity, as measured by DSC. The most likely cause for this extended duration necessity compared

to other literature is the inclusion of a lid on the graphite crucible containing the sample during trials that hindered the release of water vapor from the samples.

Explored ratios of ammonium bifluoride to uranium tetrafluoride ranged from 2:1 to 1:2 by mass (molar ratios of approximately 12:1 to 3:1). Due to large excesses of ammonium bifluoride observed with higher ratios, 1:2 mass ratios were found to produce the best DSC curves, indicating the best sample purity.

The purification process developed through the optimization of the variables described in this section improved the melting point peak and onset by over 100˚C (shifting the peak from 923.5˚C to 1032.2˚C and the onset from 915.8˚C to 1023.0˚C), which reflected the increasing purity of the salt. Analysis by XRD also revealed improved crystallinity of the purified salt when compared to the as-received salt. While XRD showed no peaks indicating oxidation, the significant improvement of melting behavior of the salt following purification indicates an improvement in salt composition. The most likely explanation of this is the removal of small amounts of oxidation in the form of uranium dioxide or uranyl difluoride that was below the detection limit of XRD analysis. The consistency that was observed with the final four sequential trials exhibits satisfaction of the secondary objective pertaining to the replicability of the process.

REFERENCES

1. Beneš, O. Thermodynamics of Molten Salts for Nuclear Applications. Doctoral Dissertation (Institute of Chemical Technology, Prague 2008).

2. Nejedly, M. & Matal, O. Studies on Components for a Molten Salt Reactor. In *Transactions of the 17th International Conference on Structural Mechanics in Reactor Technology* (Brno University of Technology, 2003).

3. Serp, J. *et al.* The molten salt reactor (MSR) in generation IV: Overview and perspectives. *Progress in Nuclear Energy* **77**, 308–319 (2014).

4. International Atomic Energy Agency. *World Nuclear Association*: *World Nuclear Performance Report 2021* (2021). https://world-nuclear.org/our-association/publications/global-trends-reports/world-nuclear-performance-report.aspx.

5. Alexander, S. *Peak Oil, Energy Descent, and the Fate of Consumerism.* SSRN: 1985677 (University of Melbourne 2012).

6. Masson- Delmotte, V. et al. IPCC Summary for Policymakers. In*: Climate Change 2021: The Physical Science Basis*. (Cambridge University 2021).

7. Global Greenhouse Gas Emissions Data. *United States Environmental Protection Agency* (2014). https://www.epa.gov/ghgemissions/global-greenhouse-gas-emissions-data.

8. Roser, M. Human Development Index (HDI). *OurWorldInData.org.* (2014). https://ourworldindata.org/human-development-index.

9. U.S. Department of Research Advisory Committee. A Technology Roadmap for Generation IV Nuclear Energy Systems. *Generation IV International Forum.* GIF-002-00 (2002).

10. U.S. Department of Research Advisory Committee. Technology Roadmap Update for Generation IV Nuclear Energy Systems. *OECD Nuclear Energy Agency* (2014). https://www.gen-4.org/gif/jcms/c_60729/technology-roadmap-update-2013.

11. Hallatt, D. B. Developing a Framework for Thermodynamic Measurements of Fluoride Salt Nuclear Fuel. Master's Thesis (Ontario Tech University, 2019).

12. Lipkina, K. Experimental Investigations of Thermodynamic Properties of the LiF-CsF Binary System and FLiNaK. Master's Thesis (Ontario Tech University, 2020).

13. Khripin, L., Poduzova, S. & Zadneprovskii, G. The UF3-UF4 System. *Russian Journal of Inorganic Chemistry* **13**, 2796–2799 (1968).

14. Friedman, H., Herbert, G. & Thoma, R. Thermal Analysis and Gradient Quenching Apparatus and Techniques for the Investigation of Fused Salt Equilibria. *Oak Ridge National Laboratory*. ORNL-3373 (1962).

15. Souček, P. *et al.* Synthesis of UF4 and ThF4 by HF gas fluorination and re-determination of the UF4 melting point. *Journal of Fluorine Chemistry* **200**, 33–40 (2017).

16. Gehin, J. & Powers, J. Liquid Fuel Molten Salt Reactors for Thorium Utilization. *Nuclear Technology* **194**, 152-161 (2016).

17. Leblanc, D. Molten Salt Reactors: A New Beginning for an Old Idea. *Nuclear Engineering and Design* **240**, 1644–1656 (2010).

18. Rosenthal, M. W., Kasten, P. R. & Briggs, R. B. Molten-Salt Reactors-History, Status, and Potential. *Nuclear Applications and Technology* **8**, 107-117 (1969).

19. Capelli, Elisa. Thermodynamic characterization of salt components for molten salt reactor fuel. Doctoral Dissertation. (University of Technology Delft, 2015).

20. Banerjee, R. H., Singh, V., Arya, A. & Banerjee, S. A comparative study of surface layer formation in Ni-based alloys with varying Cr contents exposed to high temperature fluoride environment. *Journal of Nuclear Materials* **516**, 54–62 (2019).

21. Claux, B., Beneš, O., Capelli, E., Souček, P. & Meier, R. On the fluorination of plutonium dioxide by ammonium hydrogen fluoride. *Journal of Fluorine Chemistry* **183**, 10–13 (2016).

22. Stempien, J., Ballinger, R. & Forsberg, C. An integrated model of tritium transport and corrosion in Fluoride Salt-Cooled High-Temperature Reactors (FHRs) - Part I: Theory and benchmarking. *Nuclear Engineering and Design* **310**, 258–272 (2016).

23. Benes, O., Bellmann, M. & Konings, R. Thermodynamic Assessment of the LiF-NaF-ThF4-UF4 System. *Journal of Nuclear Materials* **405**, 186–198 (2010).

24. Bahri, C., Ismall, A. & Ab Majid, A. Synthesis of thorium tetrafluoride (ThF4) by ammonium hydrogen difluoride (NH4HF2). *Nuclear Engineering and Technology* **51**, 792–799 (2019).

25. Niu, Y. *et al.* Study on the fluorination reaction of uranium tetrafluoride by nitrogen trifluoride. *Journal of Fluorine Chemistry* **230**, 1-6 (2020).

26. U.S. Department of Energy Office of Environmental Management. Characteristics of Uranium and its Compounds (2001). https://web.evs.anl.gov/uranium/pdf/UraniumCharacteristicsFS.PDF.

27. Yeamans, C. B. Dry Process Fluorination of Uranium Dioxide Using Ammonium Bifluoride. Master's Thesis (Massachusetts Institute of Technology, 2003).

28. Weaver, C., Thoma, R., Insley, H. & Friedman, H. Phase Equilibria in Molten Salt Breeder Reactor Fuels. U.S. Atomic Energy Commission. ORNL-2896 (1961).

29. Uranium Tetrafluoride SDS. *International Bio-Analytical Industries, Inc*. (2021). https://ibilabs.com/msds/uranium-compounds/uranium-fluoride-msds/.

30. Dworkin, A. S. Enthalpy of Uranium Tetrafluoride from 298-1400°K: Enthalpy and Entropy of Fusion. *J. Inorg, NucI. Chem* **34**, 135-138 (1972).

31. Pomiro, F. J., Gaviría, J. P., Bohé, A. E. & de Micco, G. Thermodynamic analysis of uranium oxides fluorination with HF(g) and F2(g). *Journal of Radioanalytical and Nuclear Chemistry* **324**, 1283–1292 (2020).

32. Wani, B. N. & Rao, U. R. K. Interfacial Reaction Between Ammonium Hydrogen Fluoride and Binary Oxides at Room Temperature. *Materials Chemistry and Physics* **33**, 165-167 (1993).

33. Yahata Tadasumi Muromura, T., Ouchi, K. & Naito, K. A Study of Ammonium Plutonium(IV) Fluorides-II. *J Inorg. Nucl. Chem* **33**, 3339–3343 (1971).

34. Mukherjee A., Awasthi A. & Krishnamurthy, N. Studies on Fluorination of Y_2O_3 by NH_4HF_2. *Thermochimica Acta* **520**, 145-152 (2011).

35. Booth, H. S., Krasny-Ergen, W., Heath, R. E. & F Lundell, G. E. Uranium Tetrafluoride. *Journal of the American Chemical Society*. **68**, 196 (1946).

36. Benz, R., Douglass, R., Kruse, F. & Penneman, R. Preparation and Properties of Several Ammonium Uranium (IV) and Ammonium Plutonium (IV) Fluorides. *Journal of Inorganic Chemistry* **2**, 799–803 (1962).

37. Penneman, R., Kruse, F., George, R. & Coleman, J. Studies of the Ammonium Fluoride-Uranium Tetrafluoride-Water System. Properties of (NH4)4UF8, (NH4)2UF6, 7NH4F*6UF4, and of U(IV) in Aqueous NH4F. *Journal of Inorganic Chemistry* **3**, 309-315 (1964).

38. Typical Alkaline Materials (Bases) for Neutralization of HF. *Honeywell* (2014). https://www.honeywell-hfacid.com/document/hf-neutralization/?download=1%20onclick=.

39. Perkins, B. Evaluation of Environmental Control Technologies for Commercial Fuel-Conversion (UF6) Facilities. *Los Alamos National Laboratory*. LA-9397-MS (1982).

40. Rampersadh, P. Removal of Hydrogen Fluoride from Gas Streams. Doctoral Dissertation (University of Witwatersrand, 2005).

41. Dillon, C. & Davies, M. Alloy Selection for Service in Hydrogen Fluoride, Hydrofluoric Acid, and Fluorine. *Nickel Institute* (2019). https://nickelinstitute.org/media/4124/alloy-selection-for-service-in-hydrogen-fluoride-hydrofluoric-acid-and-fluorine-10074.pdf.

42. Delpech, S., Cabet, C., Slim, C. & Picard, G. S. Molten Fluorides for Nuclear Applications. *Materials Today* **13**, 34–41 (2010).

43. Osborne, P., Icenhour, A. & Del Cul, G. Hydrofluoric Acid Corrosion Study of High-Alloy Materials. *U.S. Department of Energy*. ORNL/TM-2002/165 (2002).

44. Syarifuddin, F. *et al.* Effect of acid leaching on upgrading the graphite concentrate from West Kalimantan (Indonesia). in *AIP Conference Proceedings* vol. 1712 (American Institute of Physics Inc., 2016).

45. Mustika, D. *et al.* Purification of Indonesian Natural Graphite by Acid Leaching Method as Nuclear Fuel Matrix: Physical Characterization. *International Journal of Chemistry* **11**, 9 (2019).

46. Adham, K. & Bowes, G. Natural Graphite Purification Through Chlorination in Fluidized Bed Reactor. in *Extraction 2018*. 2505–2512 (Springer, Cham 2018).

47. Wani, B., Patwe, S., Rao, U. & Venkateswarlu, K. Fluorination of Oxides of Uranium and Thorium by Ammonium Hydrogenfluoride. *Journal of Fluorine Chemistry* **44**, 177–185 (1989).

48. Fedorov, P. Glass Formation Criteria for Fluoride Systems. *Inorganic Materials* **33**, 1415–1424 (1997).

49. Ronkay, F. *et al.* Melting temperature versus crystallinity: new way for identification and analysis of multiple endotherms of poly(ethylene terephthalate). *Journal of Polymer Research* **27**, 372 (2020).

50. Fischer, C. & Drummer, D. Crystallization and Mechanical Properties of Polypropylene under Processing-Relevant Cooling Conditions with respect to Isothermal Holding Time. *International Journal of Polymer Science* **2016**, 1-11 (2016).

51. Tosolin, A., Capelli, E., Konings, R., Luzzi, L. & Benes, O. Isobaric Heat Capacity of Solid and Liquid Thorium Tetrafluoride. *Journal of Chemical and Engineering Data* **64**, 3945–3950 (2019).

APPENDIX A: STANDARD OPERATING PROCEDURES

A1. Baking Out the Graphite Crucible

1. Prior to the day of a purification trial, the graphite crucible that will be used to hold the powder in the trial should be loaded into the Ni Parr reaction vessel in lab 024. The top of the vessel should then be screwed on and the hex key should be used to tighten each of the compression fittings on the top of the vessel.

2. The heating tape should then be applied to the vessel with maximum contact area ensured by the use of 3 worm gear clamps placed at the bottom, the middle, and the top of the vessel. The J-type thermocouple from the temperature controller should be placed between the heating tape and the vessel. Do not overtighten the clamps as this can damage the heating tape. The heating tape should not be overlapped.

3. Insulation should be applied around the vessel using the mineral wool tubing insulation around the outside of the vessel and a square piece of fiberglass insulation with a hole in the center for the top. The insulation should be tied closed using the copper wiring in the glovebox of 024.

4. Hit the setpoint button on the temperature controller twice and adjust the temperature to 500˚C before pressing the setpoint button one additional time. Once the temperature has been set, the heating tape can be plugged into the SDC temperature controller.

5. The heating tape should be left on for 3 hours with consistent monitoring. The glovebox gloves should be left outside of the box when not in use.

6. When the 3 hours are over, the heating tape should be unplugged from the temperature controller.

7. After 2 hours, the copper cord can be untied, and the insulation should be vented.

8. After at least 3 more hours, the vessel should be cool enough to handle, but first, check the reading of the temperature controller. If it is no longer above 45˚C, the insulation can be removed completely. The top clamp can be opened to allow the top of the vessel to be

removed once loosened with the hex key. The heating tape is not made to be frequently removed and reapplied so full removal should be avoided when possible.

9. The crucible should be removed using the extended length tweezers located in the glovebox and placed in a mason jar.

10. The mason jar should be sealed prior to removal from the 024 glovebox and relocation to the 025 glovebox.

A2. Purification of UF_4

1. Proper gowning procedure will be followed at all times including the use of a lab coat, safety glasses, and nitrile gloves. A whole-body dosimeter will be worn at all times during this work on the breast pocket of the lab coat.

2. Sample preparation will take place in the glovebox within lab 025 in Horizon 1 building, and all heating of the system will occur within the glovebox of lab 024. Within the glovebox of 024 will be a scrubber system using KOH that is designed to remove HF created by the dissociation of NH4HF2 based on the following reaction that was previously validated using TGA:

NH4HF2(s)→NH3(g)+2HF(g)

3. Approximately 175 mg of NH4HF2 sourced from Chem Impex International and 350 mg of UF4 sourced from Oak Ridge National Lab will be ground together for 15 min using a mortar and pestle (sample sizes may vary but the ratio should remain constant). This mixture will then be transferred to a 20 mm x 20 mm graphite crucible that was previously baked under argon to remove impurities. The crucible should be weighed pre and post loading to determine total sample size.

4. This crucible will then be placed in a Ziploc bag with the lid on and sealed. The bag should be placed inside of an air tight container and sealed. The crucible can then be relocated to the glovebox in 024. Note: This can be left overnight to be run the next day due to lengthy trial times.

5. Once within the glovebox, the crucible should be placed on top of a 1.5 inch stage within a Parr Instruments reaction vessel from PO #200055041. The top of the reaction vessel, which is rated for 10 bars, can then be screwed on, and the compression fittings on the top should be sealed using the hex key provided by Parr Instruments.

6. The heating tape should then be applied to the vessel with maximum contact area ensured by the use of 3 worm gear clamps placed at the bottom, the middle, and the top of the vessel. The J-type thermocouple from the temperature controller and an additional external K-type thermocouple should be placed between the heating tape and the vessel. Do not overtighten the clamps as this can damage the heating tape. The heating tape should not be overlapped.

7. Insulation should be applied around the vessel using the mineral wool tubing insulation around the outside of the vessel and a square piece of fiberglass insulation with a hole in the center for the top. The insulation should be tied closed using the copper wiring in the glovebox of 024.

8. Once insulation has been applied, the inlet and outlet tubing should be attached to the vessel to connect to the argon supply and off-gas system, respectively.

9. Argon, flown through the Setnag Gen'Air, will be used to purge the system for 20 min prior to heating at a rate of approximately .5 LPM as previously set by the flowmeter on a Rapidox 3100. Gas will exit the vessel via a ball valve on the outlet and bedirected by PTFE lines into three series connected scrubbers filled with solid KOH. The purged gas from the system is exhausted into the vacuum by the glovebox.

10. The setpoint button on the temperature controller should be pressed twice and the temperature adjusted to 100˚C before pressing the setpoint button one additional time. Once the temperature has been set, the heating tape can be plugged into the SDC temperature controller.

11. The heating tape should be left at this temperature for a total of 7 hours with consistent monitoring.

12. After 7 hours, the temperature can be increased to 480˚ at a ramp rate of 3˚C/min. This is done manually by increasing the temperature 15˚C every 5 min. Once at the top temperature, it should be left at this temperature for a total of 16 hours before being turned off.

13. 2 hours after heating has stopped, the copper cord can be untied, and the insulation should be vented.

14. After at least 3 more hours, the vessel should be cool enough to handle, but first, check the reading of the temperature controller. If it is no longer above 45˚C, the insulation can be removed completely. The top clamp can be opened to allow the top of the vessel to be removed once loosened with the hex key. The heating tape is not made to be frequently removed and reapplied so full removal should be avoided when possible.

15. The sample can be removed and visually observed. The product should be green and in the form of a puck. Residual ammonium bifluoride presents itself in the form of a grey outer layer, and oxidation can be seen in specks of black or an outer layer of black depending on severity.

16. The crucible with uranium tetrafluoride should be weighed following completion to compare its mass to the theoretical yield.

APPENDIX B: FLOW CHART OF REACTION SYSTEM

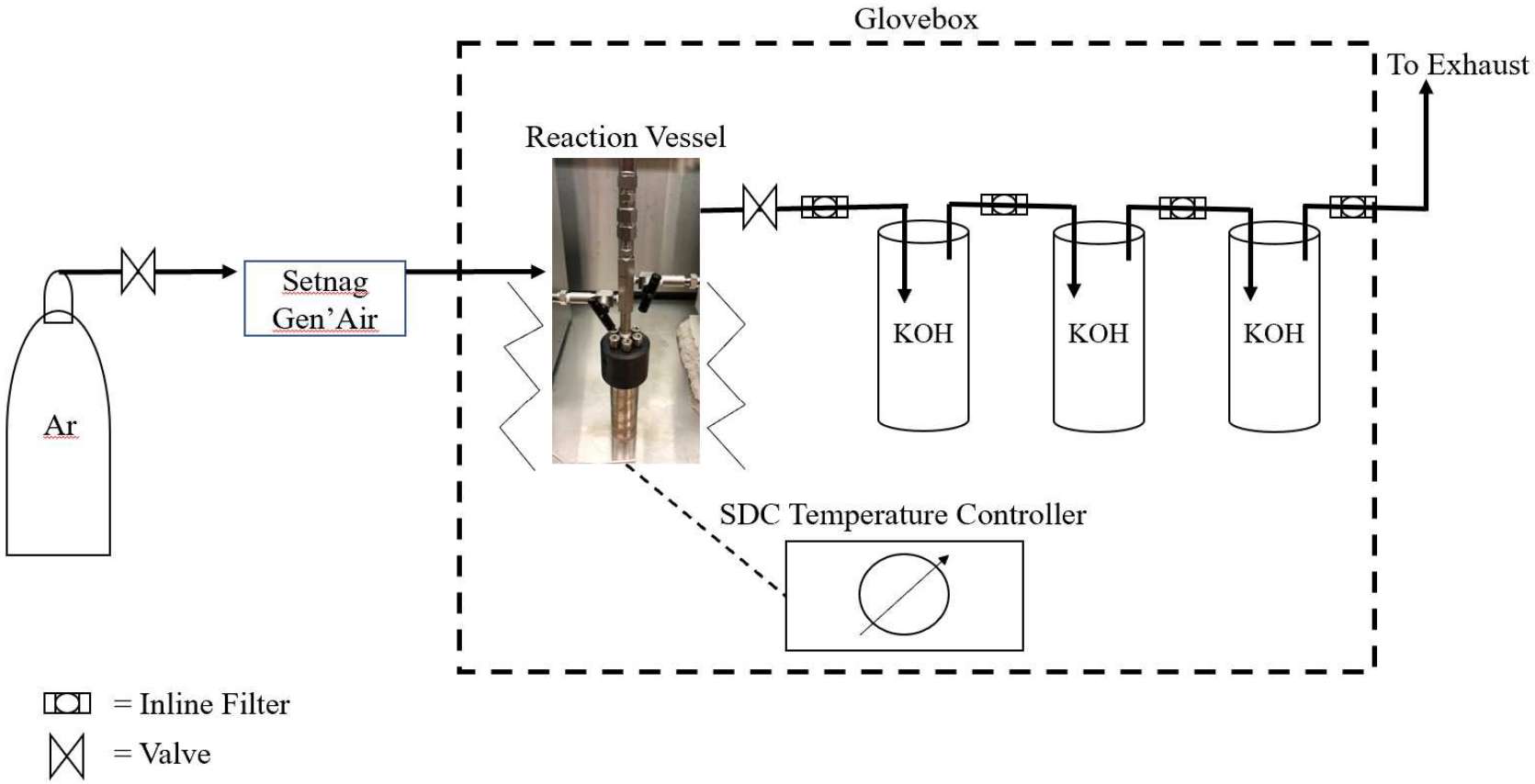

APPENDIX C: DATA FROM ICP-OES

C1. Calibration Curves in Calibration Units

Table C.1: ICP Calibration of Calcium

				Cor. Coef:
Ca 317.933		Equ: Linear Through Zero		0.995201
Sample Id	**Corrected Intensity**	**Entered Conc.**	**Calculated Cal Unit Conc.**	**% Residual Error**
Calib Blank 1	0.0	0.000	0.000	N/A
Calib Std A1	767510.8	1.000	1.742	74.18
Calib Std A2	2511217.9	5.000	5.699	13.98
Calib Std A3	4219840.6	10.000	9.576	-4.24

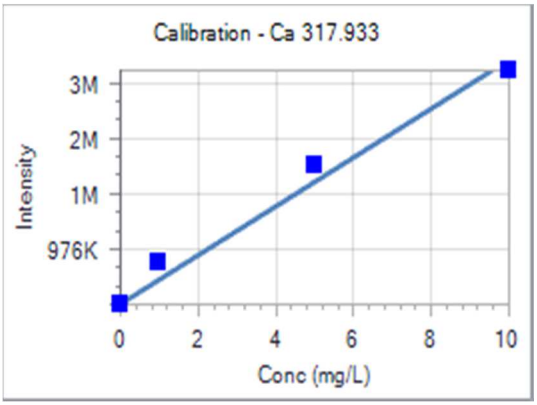

Figure C.1: Calibration curve of calcium

Table C.2: ICP Calibration of Aluminum

				Cor. Coef:
Al 396.153		Equ: Linear Through Zero		0.999865
Sample Id	**Corrected Intensity**	**Entered Conc.**	**Calculated Cal Unit Conc.**	**% Residual Error**
Calib Blank 1	0.0	0.000	0.000	N/A
Calib Std A1	1045550.0	1.000	0.923	-7.72
Calib Std A2	5498953.6	5.000	4.853	-2.93
Calib Std A3	11421882.1	10.000	10.081	0.81

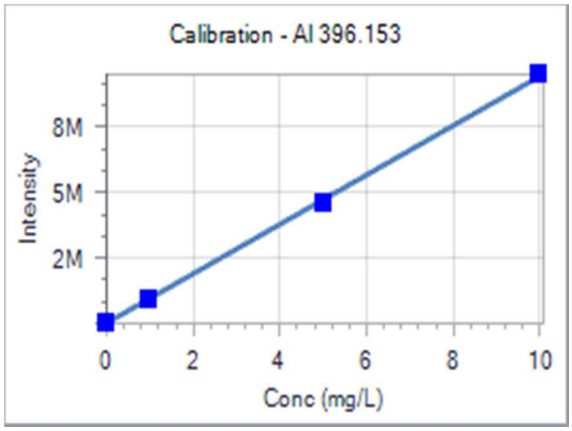

Figure C.2: Calibration curve of aluminum

Table C.3: ICP Calibration of Iron

				Cor. Coef:
Fe 238.204		Equ: Linear Through Zero		0.999995
Sample Id	**Corrected Intensity**	**Entered Conc.**	**Calculated Cal Unit Conc.**	**% Residual Error**
Calib Blank 1	0.0	0.000	0.000	N/A
Calib Std A1	1794083.8	1.000	1.026	2.62
Calib Std A2	8774363.8	5.000	5.019	0.38
Calib Std A3	17460829.0	10.000	9.988	-0.12

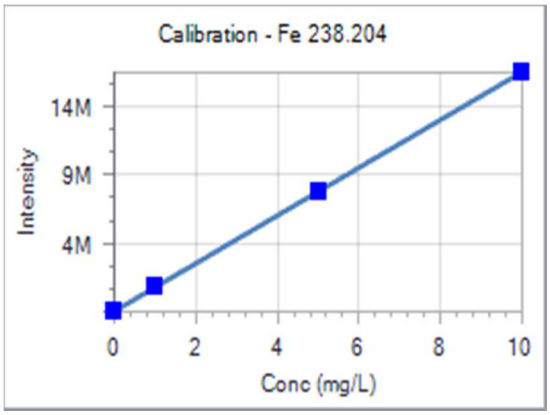

Figure C.3: Calibration curve of iron

Table C.4: ICP Calibration of Uranium

				Cor. Coef:
U 385.958		Equ: Linear Through Zero		0.999993
Sample Id	**Corrected Intensity**	**Entered Conc.**	**Calculated Cal Unit Conc.**	**% Residual Error**
Calib Blank 1	0.0	0.000	0.000	N/A
Calib Std A1	151052.8	1.000	1.014	1.41
Calib Std A2	750018.1	5.000	5.035	0.71
Calib Std A3	1486615.6	10.000	9.981	-0.19

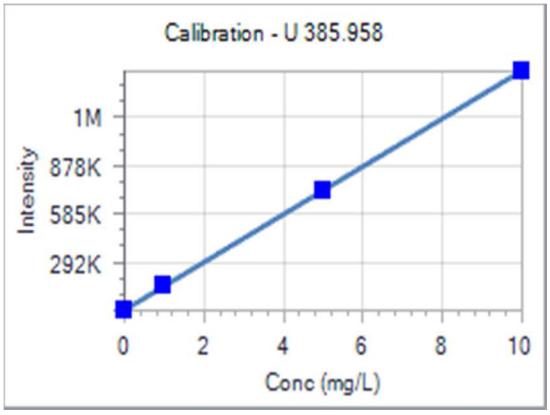

Figure C.4: Calibration curve of uranium

Table C.5: ICP Calibration of Magnesium

				Cor. Coef:
Mg 285.213		Equ: Linear Through Zero		0.999927
Sample Id	**Corrected Intensity**	**Entered Conc.**	**Calculated Cal Unit Conc.**	**% Residual Error**
Calib Blank 1	0.0	0.000	0.000	N/A
Calib Std A1	623847.0	1.000	1.065	6.49
Calib Std A2	2990198.8	5.000	5.104	2.09
Calib Std A3	5823896.7	10.000	9.941	-0.59

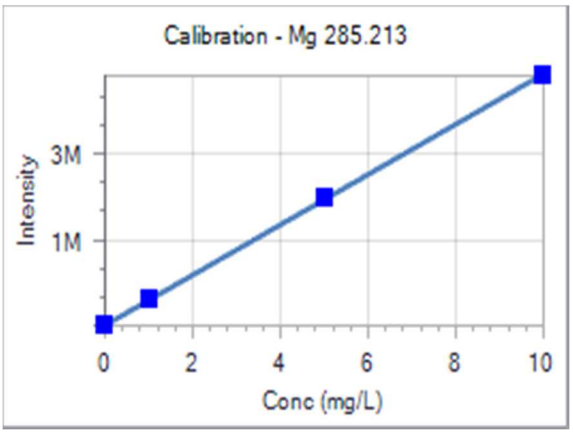

Figure C.5: Calibration curve of magnesium

Table C.6: ICP Calibration of Nickel

				Cor. Coef:
Ni 231.604		Equ: Linear Through Zero		0.999988
Sample Id	**Corrected Intensity**	**Entered Conc.**	**Calculated Cal Unit Conc.**	**% Residual Error**
Calib Blank 1	0.0	0.000	0.000	N/A
Calib Std A1	677987.5	1.000	1.042	4.15
Calib Std A2	3273599.2	5.000	5.029	0.58
Calib Std A3	6497392.0	10.000	9.981	-0.19

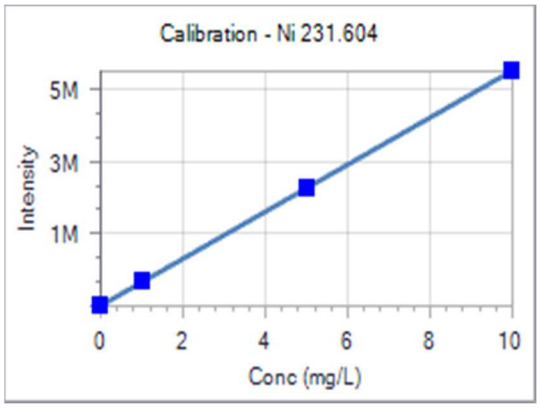

Figure C.6: Calibration curve of nickel

Table C.7: ICP Calibration of Strontium

				Cor. Coef:
Sr 407.771		Equ: Linear Through Zero		0.999985
Sample Id	**Corrected Intensity**	**Entered Conc.**	**Calculated Cal Unit Conc.**	**% Residual Error**
Calib Blank 1	0.0	0.000	0.000	N/A
Calib Std A1	19875692.7	1.000	0.973	-2.70
Calib Std A2	102241085.7	5.000	5.005	0.11

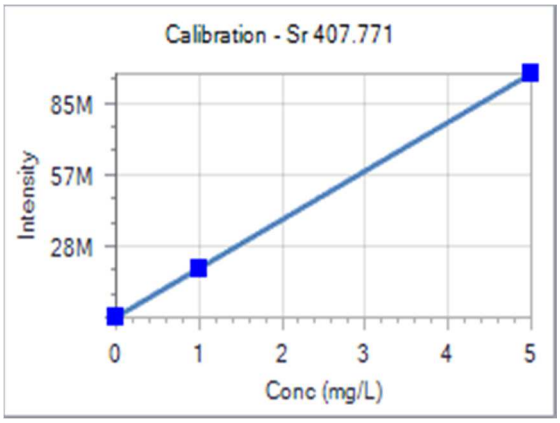

Figure C.7: Calibration curve of strontium

C2. Concentrations in Calibration Units

Table C.8: ICP-OES Results

	Sample Id	**Ca 317.933 (mg/L)**	**Al 396.153 (mg/L)**	**Fe 238.204 (mg/L)**	**U 385.958 (mg/L)**	**Mg 285.213 (mg/L)**	**Ni 231.604 (mg/L)**	**Sr 407.771 (mg/L)**
1	Calib Blank 1	0.000	0.000	0.000	0.000	0.000	0.000	0.000
2	Calib Std A1	1.000	1.000	1.000	1.000	1.000	1.000	1.000
3	Calib Std A2	5.000	5.000	5.000	5.000	5.000	5.000	5.000
4	Calib Std A3	10.000	10.000	10.000	10.000	10.000	10.000	
	Sample Id	**Ca 317.933**	**Al 396.153**	**Fe 238.204**	**U 385.958**	**Mg 285.213**	**Ni 231.604**	**Sr 407.771**
5	Calibration Curves							
	Sample Id	**Ca 317.933 (mg/L)**	**Al 396.153 (mg/L)**	**Fe 238.204 (mg/L)**	**U 385.958 (mg/L)**	**Mg 285.213 (mg/L)**	**Ni 231.604 (mg/L)**	**Sr 407.771 (mg/L)**
6	UF4-ORNL	0.226	-0.012	0.003	4.757	0.006	0.001	0.000
7	UF4-Bioanalytics	0.297	-0.005	0.000	2.661	0.005	0.001	0.000
8	UF4-Purified	0.273	-0.011	0.007	5.130	0.007	0.002	0.000
9	Water+AR	0.198	0.002	0.002	-0.001	0.004	0.002	0.001
10	Water+HCl	0.167	0.001	-0.001	0.002	0.001	0.000	-0.001
11	Water+HNO3	0.164	0.000	-0.001	-0.001	0.001	0.000	-0.001